Published in final edited form as:

Nature. 2019 July ; 571(7764): 211–218. doi:10.1038/s41586-019-1325-x.

TOX transcriptionally and epigenetically programs CD8+ T cell exhaustion

Omar Khan[1,2,3], **Josephine R. Giles**[1,2,3], **Sierra McDonald**[5,6,7], **Sasikanth Manne**[1,2], **Shin Foong Ngiow**[1,2,3], **Kunal P. Patel**[1,2,4], **Michael T. Werner**[5,7], **Alexander C. Huang**[2,3,4], **Katherine A. Alexander**[5,6,7], **Jennifer E. Wu**[1,2,3], **John Attanasio**[1,2], **Patrick Yan**[1,2], **Sangeeth M. George**[1,2], **Bertram Bengsch**[9,10], **Ryan P. Staupe**[1,2], **Greg Donahue**[5,6,7], **Wei Xu**[8], **Ravi K. Amaravadi**[8], **Xiaowei Xu**[8], **Giorgos C. Karakousis**[8], **Tara C. Mitchell**[8], **Lynn M. Schuchter**[8], **Jonathan Kaye**[11], **Shelley L. Berger**[5,6,7], **E. John Wherry**[1,2,3,*]

[1]Department of Systems Pharmacology and Translational Therapeutics, Perelman School of Medicine, University of Pennsylvania, Philadelphia, PA USA.

[2]Institute for Immunology, Perelman School of Medicine, University of Pennsylvania, Philadelphia, PA USA.

[3]Parker Institute for Cancer Immunotherapy, Perelman School of Medicine, University of Pennsylvania, Philadelphia, PA USA.

[4]Department of Medicine, Perelman School of Medicine, University of Pennsylvania, Philadelphia, PA USA.

[5]Epigenetics Institute, Perelman School of Medicine, University of Pennsylvania, Philadelphia, PA USA.

[6]Department of Cell and Developmental Biology, Perelman School of Medicine, University of Pennsylvania, Philadelphia, PA USA.

[7]Department of Genetics, Perelman School of Medicine, University of Pennsylvania, Philadelphia, PA USA.

Corresponding Author Correspondence to E. John Wherry (wherry@pennmedicine.upenn.edu).

Contributions

O.K. and E.J.W. conceived the project, designed experiments and wrote the manuscript. O.K. performed the majority of the experiments described herein and performed the *in vitro*, *in vivo*, and bioinformatics analysis. J.R.G. wrote the script to perform PSEA and, with S.M., performed pre-processing of RNA and ATAC-seq data. S.M. performed co-IP experiments for Western blot. S.F.N and K.P.P contributed to *in vivo* tumor and influenza experiments. M.T.W. performed IP experiments for mass spectrometry. A.C.H., P.Y., and S.M.G. acquired and stained human PBMC and TIL samples. J.E.W., R.P.S., and J.R.G. provided critical edits to the manuscript. All authors reviewed the manuscript.

*Lead Contact: E. John Wherry

Competing Interests

O.K. is an employee of Arsenal Biosciences. R.K.A. serves as a consultant for Sprint Biosciences, Immunacell and Array Pharmaceuticals and is a founder of Pinpoint Therapeutics. T.C.M. is an advisor to and/or receives honoraria from Aduro, Array, BMS, Incyte, Merck, Regeneron. S.L.B receives research funding from Celgene. E.J.W. receives honoraria, consulting fees and/or research support from BMS, Celgene, Dynavax, Eli Lilly, Elstar, Merck, MedImmune, Pieris, Roche, Surface Oncology, and KyMab. E.J.W. is a founder of Arsenal Biosciences. E.J.W. has a patent licensing agreement for the PD-1 pathway.

[8]Department of Pathology and Laboratory Medicine, Perelman School of Medicine, University of Pennsylvania, Philadelphia, PA USA.

[9]Department of Medicine II, Gastroenterology, Hepatology, Endocrinology, and Infectious Diseases, University Medical Center Freiburg, Germany.

[10]BIOSS Centre for Biological Signaling Studies, Freiburg, Germany,

[11]Research Division of Immunology, Department of Biomedical Sciences, Cedars-Sinai Medical Center, Los Angeles, CA USA.

SUMMARY

Exhausted $CD8^+$ T cells (T_{EX}) in chronic infections and cancer have limited effector function, high inhibitory receptor co-expression and extensive transcriptional changes compared to effector (T_{EFF}) or memory (T_{MEM}) $CD8^+$ T cells. T_{EX} are important clinical targets of checkpoint blockade and other immunotherapies. Epigenetically, T_{EX} are a distinct immune subset, with a unique chromatin landscape compared to T_{EFF} and T_{MEM}. However, the mechanisms governing the transcriptional and epigenetic development of T_{EX} remain unknown. Here, we identify the HMG-box transcription factor TOX as a central regulator of T_{EX}. TOX is largely dispensable for T_{EFF} and T_{MEM} formation, but is critical for exhaustion and without TOX T_{EX} do not form. TOX is induced by calcineurin and NFAT2 and operates in a feed-forward loop to become calcineurin independent and sustained in T_{EX}. Thus, robust TOX expression results in commitment to T_{EX} by translating persistent stimulation into a distinct T_{EX} transcriptional and epigenetic developmental program.

Following activation by antigen, naïve $CD8^+$ T cells (T_N) undergo extensive molecular rewiring into effector $CD8^+$ T cells (T_{EFF})[1]. If antigen is cleared, a subset of T_{EFF} persist, forming long-lived, self-renewing memory T cells (T_{MEM}) capable of mounting rapid recall responses[1]. In contrast, during chronic infections or cancer, this differentiation is diverted and T cells can instead become exhausted[2]. Exhausted $CD8^+$ T cells (T_{EX}) may balance partial pathogen or tumor control while restraining immunopathology. The consequence of restrained functionality, however, is disease persistence and/or progression[3,4]. T cell exhaustion is a common feature of many chronic infections and cancers in mice and humans[5–8]. Indeed, T_{EX} are a major target of checkpoint blockade in patients with cancer[9–12].

T_{EX} are characterized by the hierarchical loss of cytokine production (IL-2, TNF, IFNγ), high inhibitory receptor co-expression (PD-1, LAG3, TIGIT, etc), altered metabolism, and impaired proliferative potential and survival[2]. T_{EX} also display a distinct transcriptional program highlighted by altered use of key transcription factors (TF)[13]. Moreover, recent epigenetic analysis revealed that T_{EX} differ from T_{EFF} and T_{MEM} by ~6000 open chromatin regions[14–17], similar to differences between other major hematopoietic lineages[18]. Thus, T_{EX} are not simply a state of activation of T_{EFF} or T_{MEM}, but rather a distinct cell type. Yet, the mechanisms that initiate this T_{EX} fate commitment and epigenetic and transcriptional programming have remained elusive.

Here, we identify a requisite role for the HMG-box TF TOX in programming the early epigenetic events driving fate commitment of T_{EX}. While robustly expressed in T_{EX}, TOX is only transiently expressed at low levels during acute infections. Moreover, T_{EFF} and T_{MEM} can form without TOX whereas T_{EX} cannot. TOX is necessary and sufficient to induce major features of T_{EX}, including inhibitory receptor expression, decreased function and the expression of TFs required for T_{EX}. TOX translates early, sustained NFAT2 activity into a subsequent calcineurin-independent TOX-driven molecular and epigenetic T_{EX} program. Furthermore, TOX represses terminal T_{EFF}-specific epigenetic events while initiating key T_{EX}-specific epigenetic changes. These data identify TOX as a critical T_{EX}-programming transcriptional and epigenetic coordinator. Moreover, these observations have implications for the ontogeny of T_{EX} and therapeutic opportunities.

Transcriptional upregulation of *Tox* selectively in developing T_{EX}

We first analyzed transcription data of virus-specific $CD8^+$ T cells responding to acute (Armstrong; Arm) or chronic (clone 13; Cl-13) LCMV infection and detected considerable divergence of gene expression by day 6 post-infection (d.p.i., Fig. 1a). We hypothesized that genes with chromatin modulating capacity could drive distinct transcriptional trajectories in developing T_{MEM} and T_{EX}. Indeed, gene ontology analysis identified differentially expressed gene families with chromatin binding and TF activity (Fig. 1b). Moreover, genes within these families were differentially engaged during T cell differentiation, suggesting distinct chromatin modulators that were involved in T_{EFF}, T_{MEM} and T_{EX} differentiation (Fig. 1c, Extended Data Fig. 1a and Supplementary Table 1). Genes in cluster 1 were biased to chronic infection and included several TFs (*Stat1*, *Stat2*, *Tcf4*, *Ikzf2*) and chromatin modulators (*Tet2*, *Dnmt3a*) with roles in T cell exhaustion[19,20] as well as genes with uncharacterized functions in T_{EX} including *Setbp1*, *Kdm4a*, and *Tox* (Fig. 1d and Extended Data Fig. 1a,b). Among these, *Tox* was the most differentially expressed in developing T_{EX} *versus* T_{EFF} and T_{MEM} (Fig. 1e).

TOX is involved in the development of natural killer, innate lymphoid-like, and $CD4^+$ T cells[21,22]. Yet, the role of TOX in peripheral $CD8^+$ T cells is poorly understood. Previous network analyses found TOX to be the most differentially connected TF between T_{MEM} and T_{EX}, suggesting a prominent role in T_{EX}[13]. Moreover, chromatin accessibility of the *Tox* locus was increased in T_{EX} compared to T_{EFF}, suggesting epigenetic remodeling of *Tox* in T_{EX} (Fig. 1f). The *Tox* locus harbored a dense cluster of open chromatin regions, a feature associated with “stretch” or “super” enhancers (SEs)[23,24]. Such SEs often demarcate genes or loci involved in cell fate decisions[24]. Among loci with large stretches of open chromatin, *Tox* ranked much more highly in T_{EX} (rank = 35) compared to T_N, T_{EFF}, and T_{MEM} (rank = 91, 365, and 64 respectively) (Extended Data Fig. 1c). Together, these data provoke the hypothesis that TOX may act as a central node in the differentiation of T_{EX}.

High and sustained TOX is associated with exhaustion

TOX protein expression significantly increased by d4 of Cl-13 infection and ~80% of LCMV-specific P14 $CD8^+$ T cells expressed high TOX by d5 p.i. (Fig. 2a). Moreover, high TOX expression was sustained in >95% of T_{EX} from d15 p.i. onward and remained highly

expressed >200 days p.i. (Fig. 2a and Extended Data Fig. 2a). In contrast, although TOX was initially expressed in some T_{EFF} responding to Arm infection, expression peaked 5–6 days p.i. and was limited to ≤25% of the population. Moreover, the amount of TOX protein per cell was low and expression was transient, returning to near baseline between d8–15 p.i. (Fig 2a). Thus, high and sustained TOX was observed only during chronic infection. Notably, the difference in TOX emerged before the time when the virological outcomes diverged (~8 days p.i[25]), suggesting that viral load alone was not a primary driver of differential expression.

Whereas CD127+KLRG1- cells contained both TOX+ and TOX- cells early in Cl-13 infection, TOX- cells were enriched in the CD127-KLRG1+ subset suggesting a negative relationship between TOX and KLRG1+ terminal effector cells[26–28] (Extended Data Fig. 2b). This KLRG1+ terminal effector population is unable to generate T_{EX}, perhaps due to a lack of TCF1 and Eomes[28–30]. Indeed, TCF1 and Eomes expression was confined mainly to the TOX+ cells at d8 p.i. (Fig. 2b **and** Extended Data Fig. 2c**, top**). Although both TCF1 subsets expressed TOX later in Cl-13 infection, higher TOX correlated with higher Eomes (Fig. 2b **and** Extended Data Fig. 2c**, bottom**)[29]. TOX+ cells also had high expression of PD-1, TIGIT, LAG3, and CD160 throughout Cl-13 infection (Fig. 2c and Extended Data Fig. 2d,e). Thus, TOX expression was anti-correlated with the development of KLRG1+ terminal T_{EFF} and instead was associated with high inhibitory receptors and key T_{EX} TF.

TOX expression in the setting of other acute infections was limited to the peak of the effector phase and rapidly diminished over time (Extended Data Fig. 2f). In contrast, the majority of tumor-infiltrating $CD8^+$ T cells (TILs) in B16F10 (B16) or CT26 tumors had high TOX and a high frequency of human melanoma TILs also expressed TOX (Extended Data Fig. 2g). Additionally, in analysis of single cell RNA expression data from TILs of patients with non-small cell lung cancer (NSCLC) or hepatocellular carcinoma (HCC), *TOX* expression was limited to the T_{EX} subset (Extended Data Fig. 2h). In TILs from mice and humans, there was a strong association between high TOX and high co-expression of inhibitory receptors (Fig. 2d,e and Extended Data Fig. 2g). Finally, TOX expression in tumor-specific TILs was negatively associated with the production of inflammatory cytokines, suggesting that TOX may regulate T cell function in tumors (Extended Data Fig. 2i).

An essential role for TOX in the generation of T_{EX}

To further interrogate the role of TOX in T_{EX}, we generated $TOX^{Flox/Flox}$ $CD4^{Cre}$ P14 mice (cKO). Naïve TOX cKO P14 T cells were mixed 1:1 with WT P14 cells and adoptively transferred into new mice (Extended Data Fig. 3a,b). In chronic infection, TOX cKO P14 cells mounted an initial response, but then rapidly declined in number and were not sustained past d15 p.i., unlike WT P14 cells that persisted (Fig. 3a and Extended Data Fig. 3c). This decline was not due to rejection as TOX+ escapees could readily be detected long-term and both TOX cKO and WT P14 cells initially proliferated similarly based on Ki-67 (Extended Data Fig. 3d,e). Moreover, TOX cKO cells responding to acutely resolved LCMV Arm generated robust T_{EFF} and T_{MEM} cells detectable for >30 days (Fig. 3a). Thus, TOX cKO $CD8^+$ T cells were not intrinsically unable to form $CD8^+$ T cells that could persist

following acute infection, including T_{MEM}, but rather had a specific defect in T_{EX} generation.

TOX cKO P14 cells generated more KLRG1+CD127- T_{EFF} in both acute and chronic infection (Fig. 3b and Extended Data Fig. 3f). Yet, in Arm infection, TOX cKO cells effectively generated typical T_{MEM} populations (Extended Data Fig. 3g–k). In chronic infection, TOX cKO cells expressed lower PD-1, CD160, LAG3, and TIGIT (Fig. 3c). In contrast, 2B4 and TIM3 were increased without TOX, in agreement with previous studies that showed an anti-correlated relationship between PD-1 and TIM3 early in Cl-13 infection[31] (Fig. 3c). TOX deficiency also improved function (Fig. 3d). Because complete TOX deficiency resulted in an inability to sustain T_{EX} responses, we next asked whether conditional deletion of one allele would enhance tumor immunity. Indeed, partially TOX-deficient tumor-specific T cells controlled tumor growth significantly better than WT cells (Fig. 3e).

The establishment and maintenance of T_{EX} depends on a proliferative hierarchy mediated by TCF1, T-bet and Eomes[29–31]. We therefore examined the expression of these TFs in the absence of TOX in T_{EX}. Eomes was reduced in the absence of TOX, whereas T-bet was unaffected (Fig 3f). TCF1 expression was nearly ablated in TOX cKO $CD8^+$ T cells during chronic infection with a near absence of the TCF1+ subset of T_{EX} (Fig 3f). Notably, there was no defect in TCF1 expression by naïve TOX cKO cells and TOX cKO T_{MEM} generated after acute infection retained the ability to express TCF1 and Eomes (Extended Data Fig. 3b,h). These data suggested that a primary defect in TOX cKO T_{EX} cells was the inability to re-wire transcriptional control of TCF1 and/or Eomes after initial T_{EX} precursor development with a resulting loss of the TCF1+ subset of T_{EX}.

Transcriptional analysis of WT and $TOX^{-/-}$ P14 T cells on d8 of Cl-13 infection revealed differential expression of >3,100 genes. A major feature of these data was the upregulation of many T_{EFF}-like genes in the absence of TOX including *Klrg1, Gzma, Gzmb, Cx3cr1, Zeb2* and *Prf1* (Fig. 3g and Supplementary Table 2). In contrast, downregulated genes included *Pdcd1* and *Cd160* as well as a number of genes associated with T cell or T_{EX} progenitor biology including *Myb, Il7r, Cxcr5, Slamf6*, *Lef1*, and *Tcf7* (Fig. 3g). Indeed, in the absence of TOX in Cl-13 infection, there was strong enrichment for the signature from T_{EFF} generated during LCMV Arm infection, whereas the signature of T_{EX} precursors was depleted (Fig. 3h). These data suggested that TOX was necessary to program early transcriptional responses to Cl-13 infection. Moreover, the increased signature of short-lived KLRG1+ effectors that are incapable of giving rise to T_{EX} could relate to increased TCR signaling due to reduced inhibitory receptor expression in the absence of TOX (Fig. 3i and Extended Data Fig. 3l,m)[27,32]. Finally, enrichment of the T_{EFF} signature in $Tox^{-/-}$ cells was not due solely to the loss of *Tcf7* expression, as only a minor proportion of the total transcriptional signature can be accounted for by the signature of $Tcf7^{-/-}$ T cells (Extended Data Fig. 3n)[31]. Collectively, these findings suggest that TOX promotes the generation of T_{EX} by fostering key developmental hallmarks of exhaustion while repressing development of the KLRG1+ T_{EFF} lineage.

Calcium signaling and NFAT2 are required for inducing but not sustaining TOX

In $CD4^+CD8^+$ (DP) thymocytes, TOX expression depends on calcineurin signaling[33]. Indeed, ionomycin (Iono) induced TOX in naïve $CD8^+$ T cells, whereas phorbol myristate acetate (PMA) alone or with Iono failed to induce TOX (Fig. 4a). These results suggested that TOX expression in mature $CD8^+$ T cells was primarily regulated by calcineurin-mediated signaling. Calcineurin signaling operates primarily through NFAT proteins[34] and analysis of NFAT1[35] and NFAT2[36] DNA binding data from T_{EFF} indicated that both were capable of binding to the *Tox* locus (Fig. 4b). Since *Nfatc1* (NFAT2) is differentially expressed in T_{EX} *versus* T_{EFF} and T_{MEM} (Extended Data Fig. 4a), we focused on this NFAT. Retroviral (RV) expression of a constitutively active and nucleus-restricted mutant (CA-NFAT2) induced TOX *in vitro*, whereas WT NFAT2 did not (Fig. 4c and Extended Data Fig. 4b)[37]. Moreover, NFAT2 cKO P14 T cells ($NFAT2^{Flox/Flox}$ $CD4^{Cre}$ P14) failed to express TOX *in vivo* during Cl-13 infection (Fig. 4d and Extended Data Fig. 4c). Indeed, NFAT2-deficient P14 T cells phenocopied TOX cKO P14 cells and failed to generate T_{EX} precursors, instead producing T_{EFF} with increased KLRG1 and lower PD-1 and TCF1 (Fig. 4d). To complement the NFAT2 cKO approach, Cl-13 infected mice containing WT P14 T cells were treated with the calcineurin inhibitor FK506 starting at d3 p.i. Treatment between d3–7 p.i. had minimal effect on overall T cell activation, as measured by CD44 expression, but significantly reduced TOX expression (Fig. 4e and Extended Data Fig. 4d). Moreover, P14 cells from mice treated with FK506 phenocopied TOX-deficient T cells based on high KLRG1, low Eomes, and lack of TCF1 (Fig. 4e). RV expression of TOX in NFAT2-deficient T cells restored PD-1 and expression of other inhibitory receptors, increased Eomes and TCF-1, and significantly reduced KLRG1 (Fig. 4f and Extended Data Fig. 4e). Thus, calcineurin and NFAT2 are required to induce TOX. However, enforced TOX expression in NFAT2-cKO cells can restore early T_{EX} differentiation demonstrating a key role for TOX as an inducer of T_{EX} differentiation downstream of NFAT2.

We next tested whether continuous calcium and NFAT signaling were required for the sustained TOX expression once exhaustion was established. Treatment with FK506 or cyclosporin A (CsA) between d25–29 of chronic infection reduced Ki-67 in T_{EX} (Fig. 4g and Extended Data Fig. 4f,g), as expected due to the requirement of TCR signaling to drive the proliferative hierarchy of T_{EX}[29]. Although treatment of established T_{EX} *in vivo* slightly enriched for the progenitor T_{EX} subset ($TCF1^{HI}$), there was little impact on TOX expression and essentially all virus-specific T_{EX} remained TOX+ (Fig. 4g and Extended Data Fig. 4g). Moreover, expression of PD-1 and Eomes remained essentially unchanged (Fig. 4g and Extended Data Fig. 4g). These data indicate that although initial TOX induction requires NFAT2, TOX expression and the TOX-dependent T_{EX} program become independent of calcineurin signaling once established.

A program of exhaustion induced by TOX

We next tested whether TOX was sufficient to drive exhaustion. RV TOX expression *in vitro* reduced cytokine production while increasing PD-1 (Fig. 5a,b). To test whether these TOX-

induced changes were durable *in vivo*, P14 T cells were transduced with *Tox* RV and transferred into LCMV Arm-infected mice. *In vivo*, TOX expression reduced KLRG1+ T_{EFF}, increased inhibitory receptors, and reduced function (Extended Data Fig. 5a–c). Moreover, RV-expressed TOX reduced expression of T-bet and increased TCF1 (Extended Data Fig. 5d). Thus, enforced TOX expression drove key features of T_{EX}, skewed differentiation away from T_{EFF} and T_{MEM}, and sustained these effects for >30 days (Extended Data Fig. 5e,f). RNA-seq of RV-transduced $CD8^+$ T cells *in vitro* revealed downregulation of T_{MEM} signatures and an upregulation of genes involved in exhaustion (Fig. 5c, Extended Data Fig. 5g, and Supplementary Table 3)[13,38]. Indeed, many key individual exhaustion genes such as inhibitory receptors (*Pdcd1*, *Lag3*, *Ctla4*) and transcription factors (*Nr4a2*, *Ikzf3*, *Tox2*, *Bhlhe41*) were induced by RV-mediated TOX expression *in vitro* whereas memory-associated genes (*Ccr7*, *Il7r*, *Sell*) were repressed (Fig. 5d). Moreover, even in an unrelated cell type (NIH3T3 fibroblasts) TOX induced expression of multiple immune pathways including those associated with inflammatory cytokine production, T cell activation and proliferation as well as calcineurin and NFAT signaling (Fig. 5e and Extended Data Fig. 5h,i). Additionally, the transcriptional signature induced by TOX in fibroblasts enriched for the signature of *in vivo* T_{EX} (Fig. 5f, Extended Data Fig. 5j, and Supplementary Table 4). Thus, TOX was capable of inducing a transcriptional program of T_{EX} and could even do so, at least partially, in an unrelated cell type, reminiscent of data for related HMG TF TCF1 that can induce naïve T cell genes in fibroblasts[39].

Epigenetic programming of T_{EX} by TOX

Recently we and others demonstrated that T_{EX} have a unique epigenetic landscape compared to T_N, T_{EFF} and T_{MEM}[14–17]. Thus, we next asked whether TOX regulated this epigenetic commitment of T_{EX}. In the absence of TOX there were ~4,000 regions that changed in chromatin accessibility by ATAC-seq on d8 of Cl-13 infection. Over 70% of these changes were in intronic or intergenic regions consistent with enhancers, whereas 20% were at promoters or transcription start sites (TSS) (Extended Data Fig. 6a and Supplementary Table 5). Among these changes were increases in chromatin accessibility at genes associated with terminal T_{EFF} differentiation including *Klrg1, Gzma, Gzmb, Gzmm, Clnk, Zeb2*, and *Nr4a1* (Fig 6a,b and Extended Data Fig. 6b) suggesting that TOX represses accessibility of genes involved in T_{EFF}. In contrast, loci with reduced chromatin accessibility included *Tcf7* and other genes associated with T_{MEM} and T_{EX} progenitors, including *Ccr7, Slamf6, Bach2*, and *Ikzf2* (Fig. 6a,c and Extended Data Fig. 6c). Indeed, loci with significantly reduced accessibility in $TOX^{-/-}$ P14 cells were highly enriched for T_{EX}-specific sites (647/1697; 38%), whereas sites with increased accessibility were enriched in T_{EFF}-specific sites (430/2233; 19%) (Fig. 6d and Extended Data Fig. 6d). Globally, the epigenetic signature of TOX-deficient P14 cells at d8 of chronic infection was strongly enriched for the T_{EFF} signature from acute infection and depleted of the T_{EX} epigenetic signature (Fig. 6e and Extended Data Fig. 6e). Moreover, specific peaks could be identified in key genes that changed in a TOX-dependent manner including in *Klrg1*, *Zeb2*, and *Clnk*, that became more accessible in the absence of TOX and in *Tcf7*, *Bach2*, and *Ikzf2* that were reduced or lost altogether (Fig. 6b,c and Extended Data Fig. 6b,c). Notably, the epigenetic changes caused by TOX corresponded to functionally relevant events since there was a strong association of

chromatin opening with increased gene expression and *vice versa* (Extended Data Fig. 6f). Thus, these data indicate a role for TOX in both opening and closing genomic regions associated with T_{EX} or T_{EFF} differentiation respectively.

We next expressed TOX *in vitro* and examined epigenetic changes (Fig. 5a). RV-mediated TOX expression induced chromatin accessibility changes in 378 sites (Fig. 6f, Extended Data Fig. 6a and Supplementary Table 6). These epigenetic changes strongly enriched for the landscape observed in *in vivo* T_{EX}, but also overlapped with T_{EFF} possibly reflecting activation aspects of this short-term *in vitro* assay or highlighting the common epigenetic module shared between T_{EX} and T_{EFF}[14,15] (Fig. 6g and Extended Data Fig. 6g). Moreover, at least one region opened by TOX was the T_{EX}-specific enhancer −23.8kb upstream of the *Pdcd1* TSS indicating that at least some exhaustion-specific epigenetic changes can be induced *in vitro* by TOX[14,15] (Extended Data Fig. 6h).

To investigate the mechanism by which TOX induced T_{EX}-related epigenetic changes, we identified proteins bound to TOX using immunoprecipitation followed by mass spectrometry (MS) (Extended Data Fig 6i). MS identified proteins involved in chromatin organization and remodeling, RNA processing and translation, as well as DNA replication as TOX binding partners (Extended Data Fig 6j, and Supplementary Table 7). Network analysis identified the HBO1 complex, involved in histone H4 and H3 acetylation, as a major set of TOX-bound proteins (Fig. 6h,i). Indeed, four members of the histone H4-targeting HBO1 complex (Kat7, Ing4, mEaf6, Jade2) were identified by MS[40,41] (Fig. 6h,i and Supplementary Table 7). Co-immunoprecipitation confirmed that TOX interacted with Kat7, the acetyl transferase component of the HBO1 complex[40,41] (Fig. 6j). TOX also bound proteins involved in repressive epigenetic events including Dnmt1, Leo1/Paf1, and Sap130/Sin3a indicating interactions with proteins involved in both closing and opening of chromatin (Fig. 6h and Supplementary Table 7). Thus, TOX can bind and likely recruit diverse sets of chromatin remodeling proteins.

Finally, we reasoned that TOX might modulate epigenetic accessibility and indirectly impact gene expression by altering the network of TFs and their targets in T_{EX}. Indeed, PageRank network analysis[42] of transcriptional and epigenetic data revealed that *Tox*$^{-/-}$ T cells were negatively enriched for multiple TF networks downstream of TCR signaling (Fos, Jun, Stat, Batf families) including NFAT2 (Fig. 6k). Moreover, TF networks associated with transcriptional regulation (Nr1d2, Atf3, Bcl6, Sox4) and maintenance of cellular stemness (Nanog, Sox2)[43] were also lost in TOX-deficient T cells (Fig. 6k). Together, these data suggest a model where TOX, working with other TFs, is central to an epigenetic and transcriptional regulatory cascade that orchestrates the development of T_{EX}.

Discussion

Here we demonstrate a major role for TOX as the key inducer of canonical features of exhaustion and initiator of the T_{EX}-specific epigenetic program. These findings have several potential implications. First, TOX expression and the molecular events controlled by TOX could aid in more accurately detecting, quantifying and evaluating T_{EX}. Notably, recent CyTOF studies of human $CD8^+$ T cells, found TOX expression in the vast majority of T_{EX}

in HIV and lung cancer[38]. Second, these studies point to key molecular underpinnings of exhaustion relevant for reversibility and re-invigoration by immunotherapies including PD-1/PD-L1 blockade[10–12,14,44–46]. TOX or TOX-dependent events including epigenetic landscape programming may be a major reason for this developmental inflexibility of T_{EX} even following PD-1 blockade[14] suggesting potential therapeutic strategies based on TOX manipulation. Finally, these data support the notion that T_{EX} are a distinct cell type from T_{EFF} or T_{MEM}[14–17] and provide a molecular mechanism for this divergent path of differentiation.

Our observations suggest a model where TOX is a primary regulator of T_{EX} similar to other developmental programmers in immune cells[47–50]. Collectively, these data demonstrate that TOX is required for the development of T_{EX}, though other TFs are also clearly involved. The identification of an epigenetic programming mechanism for T_{EX} also suggests novel therapeutic possibilities based on modulation of TOX and/or the TOX-dependent epigenetic changes in T_{EX}.

METHODS

Mice

Mice were maintained in a specific-pathogen-free facility at the University of Pennsylvania (UPenn). Experiments and procedures were performed in accordance with the Institutional Animal Care and Use Committee (IACUC) of UPenn. Mice of the following genotypes were on a C57BL/6J background and bred at UPenn or purchased from Jackson Laboratory: WT P14, $TOX^{Flox/Flox}$ $CD4^{Cre}$ P14, $TOX^{-/-}$ P14, and $NFAT2^{Flox/Flox}$ $CD4^{Cre}$ P14. $TOX^{Flox/Flox}$ and $TOX^{-/-}$ mice were kindly provided by Jonathan Kaye[51]. For experiments with CT26 tumors, BALB/c mice were used and ordered from Charles River. For all experiments mice were age and sex-matched and male and female mice between 6–8 weeks of age were randomly assigned to experimental groups.

Naïve lymphocyte isolation and adoptive T cell transfer

T cell receptor transgenic $GP^{33–41}$ specific $CD8^+$ T cells (P14) were isolated from the peripheral blood of donor mice using gradient centrifugation with Histopaque-1083 (Sigma-Aldrich). For experiments using LCMV infection, WT P14 cells were mixed 1:1 with congenically disparate P14 cells of the desired genotype ($TOX^{Flox/Flox}$ $CD4^{Cre}$ P14, $TOX^{-/-}$ P14, or $NFAT2^{Flox/Flox}$ $CD4^{Cre}$ P14) and a total of 500 naïve cells were adoptively transferred by tail-vein injection into 6–8-week-old recipient mice 1–5 days prior to infection. Recipients were of a third congenic background to allow distinguishing of both donor populations from the host T cells. Naïve WT and TOX cKO P14 cells had similar baseline activation and expression of inhibitory receptors, enabling a direct comparison (Extended Data Fig. 3b). For experiments monitoring only WT P14 responses, 500 cells were transferred. Previous reports have shown that adoptive transfer of 500 P14 T cells prior to LCMV Cl-13 or Arm infection does not impact viral load or pathogenesis[4,52,53]. For LCMV experiments, mice were not depleted of $CD4^+$ T cells using GK1.5 antibody prior to infection. For experiments with influenza, *Listeria monocytogene*s (LM), or vesicular

stomatitis virus (VSV) infection, 5,000 P14 (influenza, LM) or OT-I (VSV) $CD8^+$ T cells were adoptively transferred prior to infection.

Viral infections, bacterial infections, and treatments

LCMV strains Armstrong (Arm) and clone-13 (Cl-13) were propagated and titers were determined as previously described[53]. C57BL/6J mice were infected intraperitoneally (i.p.) with 2×10^5 plaque-forming units (PFU) of LCMV Arm or intravenously (i.v.) with 4×10^6 PFU LMCV Cl-13. For other experiments, mice were infected with 2×10^6 PFU VSV-OVA (i.v.) or 1×10^4 colony-forming units (CFU) LM-GP33 (i.p.). For influenza infection, mice were anesthetized with isofluorane and ketamine prior to intranasal administration of 50 $TCID_{50}$ PR8-GP33 (H1N1 strain) in 30μl of PBS. FK506 (Prograf, Astellas Pharma US) was prepared for injection by diluting to 1.5mg/ml in PBS. Diluted FK506 was administered s.c. at a dose of 10mg/kg from d3–7 or d25–29 of LCMV Cl-13 infection[54]. Cyclosporin A (CsA, Sigma-Aldrich) was prepared by diluting in sunflower oil (Sigma-Aldrich). 40mg/kg of diluted CsA was administered IP daily for duration of treatment. For control treatments, PBS was administered s.c.

Retroviral transduction, *in vitro* differentiation, and cell transfer

For retroviral (RV) transduction, $CD8^+$ T cells were enriched from spleens of donor mice using an EasySep magnetic negative selection kit (Stem Cell Technologies) and transduced as described previously[55]. In brief, cells were resuspended at 10^6/ml in "complete RPMI (cRPMI)": RPMI 1640 supplemented 10% FBS, 50μM β-mercaptoethanol, 100U/ml penicillin, 100U/ml streptomycin, non-essential amino acids (Invitrogen), sodium pyruvate (Invitrogen), and HEPES buffer (Invitrogen). 3×10^6 T cells were plated in wells of a 12 well cluster dish and activated for 18–24 hours with 1ug/ml αCD3ε (145–2C11, BioLegend) and 0.5ug/ml αCD28 (37.51, BioLegend) in the presence of 100U/ml recombinant human IL-2 (Peprotech). Following activation, cells were resuspended at 3×10^6/ml in cRPMI, plated in a well of a 6 well plate and transduced with MigR1-based RV viruses in the presence of polybrene (4μg/ml) by spin infection (2000 *x g* for 75 minutes at 32°C). RV supernatants were produced by co-transfecting HEK293T cells with an RV expression plasmid and pCL-Eco packaging plasmid using Lipofectamine3000 (Invitrogen).

For *in vitro* experiments, transduced T cells were expanded and differentiated into effector T cells[35] by culturing in cRPMI in the presence of IL-2 (100U/ml) for 5 additional days. Restimulations were performed by incubating cells with biotinylated anti-CD3ε (1μg/ml, 145–2C11, BioLegend) and anti-CD28 (0.5μg/ml, 37.51, BioLegend) for 5 minutes followed by addition of 25μg/ml streptavidin (Invitrogen) for 5 hours in a 37°C incubator.

For experiments involving the transfer of transduced P14 T cells into animals, mice were infected with LCMV Arm or Cl-13 on the same day as transduction. Twenty-four hours after transduction, GFP+ cells were sorted to >98% purity and transferred i.v. into infected hosts.

Ectopic tumor models, cell transfers, and area measurements

B16-F10, B16-F10-GP33 melanoma, and CT26 colon carcinoma cell lines were purchased from ATCC. Tumor cells were maintained at 37°C in DMEM medium supplemented with

10% FBS, 100U/ml penicillin, 100U/ml streptomycin, and 2mM L-glutamine. 2×10^5 tumor cells were injected subcutaneously (s.c.) in flank of mice. To measure antigen-specific T cell responses, P14 cells were isolated from spleens of naïve mice and activated as described above for RV transduction. Activated cells were passaged every 24 hours and plated at 3×10^6 in 3ml cRPMI with 100U/ml recombinant human IL-2 per well of a 6-well plate. 72 hours following activation, 1×10^6 cells were transferred intravenously per tumor-inoculated animal. T cell transfers were performed 5 days following tumor inoculation. Tumor size was measured using digital calipers every 48 hours following inoculation.

Plasmids and cloning

Retroviral vectors encoding TOX were generated by first amplifying Gateway cloning compatible inserts from an ORF clone (Origene MR208435). PCR products were purified (PCR Purification Kit, Qiagen) and subcloned into pDONR221 using BP clonase (Invitrogen) following manufacturer instructions. Entry clones were subsequently cloned into a Gateway-compatible MigR1 vector using LR clonase (Invitrogen). WT-NFAT2 and CA-NFAT2 RV plasmids were gifts from Anjana Rao (Addgene plasmids #11101 and #11102).

Preparation of cell suspensions and restimulations

Following infection or tumor challenge, $CD8^+$ T cells were isolated from spleen and draining lymph nodes by cutting samples into small pieces and homogenizing against a 70μm cell strainer. Cells were run through cell strainer and red blood cells were lysed in ACK lysis buffer (Thermo Fisher Scientific) for 5 minutes. The cell suspension was then washed in PBS and passed through a 70μm cell strainer an additional time. Lungs and tumors were cut into small pieces using surgical scissors and digested for 1 hour at 37°C in RPMI 1640 medium supplemented with 5% FBS, 100U/ml DNaseI (Sigma-Aldrich) and 0.2mg/ml collagenase IV (Sigma-Aldrich). Samples were subsequently mechanically disrupted against a 70μm filter and washed with PBS. Red blood cells were lysed in ACK lysis buffer for 5 minutes and samples were re-filtered through a 70μm strainer. To assess cytokine and effector molecule production, 2×10^6 cells were plated in 200μl cRPMI in wells of a flat-bottom 96 well dish and incubated with $GP^{33–41}$ peptide in the presence of protein transport inhibitors (GolgiStop and GolgiPlug, BD Biosciences) for 5 hours at 37°C.

Human sample collection and staining

Normal donor peripheral blood samples (n=10, male and female donors from the ages of 18–39) were obtained from Cellular Technology, Inc. Human melanoma tumor and PBMC samples were collected from Stage III and Stage IV melanoma patients under University of Pennsylvania Abramson Cancer Center's melanoma research program tissue collection protocol UPCC 08607 in accordance with the Institutional Review Board. Tumor samples were procured from the operating room and processed the same day using manual dissociation into single cell suspension. Tumor samples were then frozen immediately using standard freeze media, and stored in liquid nitrogen. All human samples were processed and stained as previously described[56].

Flow cytometry and cell sorting

Antibodies were procured from BioLegend: CD44 (IM7), CD62L (MEL-14), CD127 (A7R34), T-bet (4B10), PD-1 (RMP1–30), CD160 (7H1), TIM3 (RMT3–23), CD3ε (17A2), TNFα (MP6-XT22), CD8α (53–6.7), CD4 (RM4–5), CD45.1 (A29), CD45.2 (104); Miltenyi Biotec: TOX (REA473); Southern Biotech: KLRG1 (2F1); eBioscience: Eomes (Dan11mag), 2B4 (eBio244F4), IFNγ (XMG1.2), Granzyme B (GB11), B220 (RA3–6B2); or from BD Biosciences: TIGIT (1G9), LAG33 (C9B7W), TCF1 (S33–966), 2B4 (2B4), Ki-67 (B56). Live cells were discriminated by staining with Zombie NIR dye (BioLegend). Intracellular and nuclear staining of cytokines, effector molecules, and transcription factors was performed using the FoxP3/Transcription Factor Staining Buffer Set (eBioscience) in accordance with the manufacturer's protocol. Flow cytometry data were acquired on a BD LSR II instrument and cell sorting was performed on a BD FACSAria enclosed within a laminar flow hood. Data were analyzed using FlowJo software (TreeStar).

Microarray analysis

Microarray data (GSE41867)[13] were processed as previously described[13,14]. Genes with chromatin modulating function were identified by compiling gene lists retrieved from gene ontology associations (GO molecular functions: chromatin binding, nucleic acid binding, nucleotide binding and PANTHER protein classes: DNA binding protein, chromatin binding protein), the EpiFactors database[57], and previously identified chromatin modulators[58] (**Extended Data Table 9**).

RNA and ATAC-seq sample preparation and sequencing

To assess the transcriptional and epigenetic impact of TOX deletion in T cells, 250 WT and 250 $TOX^{-/-}$ naïve $CD44^{LOW}CD62L^{HI}$ P14 cells sorted from peripheral blood of donors, mixed, and co-transferred into WT mice. Recipients were subsequently infected with LCMV Cl-13 and splenocytes were harvested 8 days following infection. Ten spleens were pooled for each of the 3 replicates prior to processing, $CD8^+$ T cell enrichment (using EasySep $CD8^+$ T cell negative selection kit, Stem Cell Technologies), and staining of single cell suspensions. 1×10^5 WT and $TOX^{-/-}$ P14 cells were sorted to a purity of >98% for each replicate. In ectopic and enforced expression experiments, *in vitro* differentiated $CD8^+$ T cells transduced with TOX+GFP or control GFP only (>2 biological replicates each) were sorted on GFP expression 6 days following initial activation to a purity of >98%. NIH3T3 cells were transduced with TOX+GFP or control GFP only RV viruses and cultured for 48 hours prior to cell sorting. To extract RNA, 50,000 cells were resuspended in buffer RLT supplemented with β-mercaptoethanol and processed with a RNeasy Micro Kit (Qiagen) as per the manufacturer's instructions. Total RNA libraries were prepared using a Pico Input SMARTer Stranded Total RNA-Seq Kit (Takara). Extracted RNA and libraries were assessed for quality on a TapeStation 2200 instrument (Agilent). ATAC libraries were generated as described with minor changes[59]. Briefly, nuclei from 50,000 cells were isolated using a lysis solution composed of 10mM Tris-HCl, 10mM NaCl, 3mM $MgCl_2$, and 0.1% IGEPAL CA-630. Immediately following cell lysis, nuclei were pelleted in low-bind 1.5ml tubes (Eppendorf) and resuspended in TD Buffer with Tn5 transposase (Illumina). Transposition reaction was performed at 37°C for 45 minutes. DNA fragments were purified from enzyme

solution using MinElute Enzyme Reaction Cleanup Kit (Qiagen). Libraries were barcoded (Nextera Index Kit, Illumina) and amplified with NEBNext High Fidelity PCR Mix (New England Biolabs). Library quality was assessed using a TapeStation instrument. RNA and ATAC libraries were quantified using a KAPA Library Quantification Kit and sequenced on an Illumina NextSeq 550 instrument (150bp, paired-end) on high-output flowcells.

RNA-seq data processing and analysis

FASTQ files were aligned using STAR 2.5.2a against the mm10 murine reference genome. The aligned files were processed using PORT gene-based normalization (https://github.com/itmat/Normalization). Differential gene expression was performed with Limma. Limma-voom was used to identify transcripts that were significantly differentially expressed between experimental groups using an adjusted p-value <0.05.

ATAC-seq data processing and analysis

The script used for processing raw ATAC-seq FASTQ data is available at the following GitHub repository: https://github.com/wherrylab/jogiles_ATAC. In brief, samples were aligned to mm10 reference genome with Bowtie2. Unmapped, unpaired, and mitochrondrial reads were removed using samtools. ENCODE Blacklist regions were removed (https://sites.google.com/site/anshulkundaje/projects/blacklists). PCR duplicates were removed using Picard. Peak calling was performed with MACS2 with a FDR q-value = 0.01. A union peak list for each experiment was created by combining all peaks in all samples; overlapping peaks were merged using bedtools *merge*. The number of reads in each peak was determined with bedtools *coverage*. Differentially expressed peaks were identified following DESeq2 normalization using a FDR cutoff of <0.05.

Super enhancers were identified by running the ROSE algorithm (https://bitbucket.org/young_computation/rose) on normalized ATAC-seq data previously generated from naïve, effector, memory, or exhausted $CD8^+$ T cells[14]. Stitching distance was set to 12.5kb and TSS exclusion to 2.5kb.

The scripts for peak set enrichment are available at:

https://github.com/wherrylab/jogiles_ATAC. In brief, bedtools intersect was used to find overlapping peaks between the experiment and peak set of interest. Peak names between the experiment and peak set of interest were unified using custom R scripts. GSEA was used to calculate enrichment scores.

Taiji/PageRank network analysis

The Taiji pipeline integrates diverse datasets to identify master regulators, including genome-wide expression profile and chromatin state. Analysis was performed on RNA-seq and ATAC-seq data generated from WT and $TOX^{-/-}$ P14 T cells following 8 days of infection with Cl-13 (as described in figures 3 and 6, respectively). Herein, we have implemented the pipeline described previously (http://wanglab.ucsd.edu/star/taiji)42. Briefly, ATAC-seq peaks were called by MACS2 v2.1.1 to annotate genome-wide regulatory elements and the regulatory elements are assigned to their nearest genes. Known TF motifs

are scanned in open chromatin region within each regulatory element to pinpoint the putative binding sites. TFs with putative binding sites in promoters or enhancers are then linked to their target genes to form a network. As part of Taiji pagerank analysis, a personalized PageRank algorithm is used to assess the importance of TFs in the network and Ranks are calculated for each TF based on epigenetic and RNA expression data. The normalized ranks are then compared across conditions by calculating fold change and top TFs are chosen using a cutoff of 1.5x above mean. These TFs are finally visualized in a heatmap.

Immunoprecipitation and immunoblotting

Immunoprecipitation (IP) was performed as previously described[60]. Briefly, 5×10^6 EL4 cells were lysed in immunoprecipitation buffer (20 mM Tris, pH 7.5, 137 mM NaCl, 1 mM $MgCl_2$, 1 mM $CaCl_2$, 1% NP-40, 10% glycerol) supplemented with 1:100 HALT protease and phosphatase inhibitor cocktail (Thermo Scientific) and benzonase (Novagen) at 12.5 U/ml. Lysates were rotated at 4°C for 60 minutes. Subsequently, antibody-conjugated Dynabeads (Invitrogen) were added and samples were incubated at 4°C overnight on a rotating platform. Beads were collected by magnet and samples were washed five times with immunoprecipitation buffer. Samples were then resuspended in NuPAGE loading dye (ThermoFisher), incubated at 95°C for 5 minutes and analyzed by Western blotting. The following antibodies were used for IP: TOX (ab155768, Abcam) and Kat7 (ab70183, Abcam) and Western blot: TOX (TXRX10, eBioscience), Kat7 (ab70183, Abcam), H3K4me1 (ab8895, Abcam), H3K27me3 (ab6002, Abcam), H3K9ac (39918, Active Motif), H3K27ac (ab4729, Abcam), H4 (07–108, Millipore), and H4ac (06–866, Millipore).

Immunoprecipitation, LC-MS/MS, and analysis

We used EL4 thymoma cells that express high levels of TOX and have been used previously to model some features of T_{EX}[15]. EL4 cell nuclear extract was prepared as described[61]. Briefly, cells were incubated in hypotonic buffer (10mM Tris-Cl, pH 7.4, 1.5mM MgCl2, 10mM KCl, 25mM NaF, 1mM Na_3VO_4, 1mM DTT, and Roche protease inhibitor cocktail) for 3 minutes. Cell pellets were subsequently spun down, resuspended in hypotonic buffer, and homogenized with 5 strokes of a Dounce homogenizer. Nuclei were collected by centrifugation and resuspended in extraction buffer (50mM Tris-Cl, pH 7.4, 1.5mM $MgCl_2$, 20 % glycerol, 420mM NaCl, 25mM NaF, 1mM Na_3VO_4, 1mM DTT, 400 U/ml DNase I, and protease inhibitor cocktail). Samples were incubated for 30 minutes at 4°C on a rotating platform. Extracts were diluted 3:1 in buffer containing 50mM Tris-Cl, pH 7.4, 1.5mM $MgCl_2$, 25mM NaF, 1mM Na_3VO_4, 0.6% NP-40, 1mM DTT, and protease inhibitor cocktail. Immunopurification was carried out on 1mg of nuclear extract using a magnetic co-IP kit (ThermoFisher) with 40μg anti-TOX (Abcam, ab155768) or control IgG antibody as per the manufacturer's instructions.

Liquid chromatography tandem mass spectrometry (LC-MS/MS) analysis was performed by the Proteomics and Metabolomics Facility at the Wistar Institute using a Q Exactive Plus mass spectrometer (ThermoFisher) coupled with a Nano-ACQUITY UPLC system (Waters). Samples were digested in-gel with trypsin and injected onto a UPLC Symmetry trap column (180 μm i.d. × 2 cm packed with 5 μm C18 resin; Waters). Tryptic peptides were separated by reversed phase HPLC on a BEH C18 nanocapillary analytical column (75 μm i.d. × 25

cm, 1.7 μm particle size; Waters) using a 95 minute gradient formed by solvent A (0.1% formic acid in water) and solvent B (0.1% formic acid in acetonitrile). A 30-min blank gradient was run between sample injections to minimize carryover. Eluted peptides were analyzed by the mass spectrometer set to repetitively scan m/z from 400 to 2000 in positive ion mode. The full MS scan was collected at 70,000 resolution followed by data-dependent MS/MS scans at 17,5000 resolution on the 20 most abundant ions exceeding a minimum threshold of 20,000. Peptide match was set as preferred, exclude isotopes option and charge-state screening were enabled to reject singly and unassigned charged ions. Peptide sequences were identified using MaxQuant 1.5.2.8. MS/MS spectra were searched against a UniProt human protein database using full tryptic specificity with up to two missed cleavages, static carboxamidomethylation of Cys, and variable oxidation of Met and protein N-terminal acetylation. Consensus identification lists were generated with false discovery rates of 1% at protein, and peptide levels. To generate a list of statistically significant hits, resulting iBAQ protein values from MaxQuant output were analyzed using the MiST scoring system[62], which accounts for protein abundance, specificity, and reproducibility across 3 biological replicates. STRING protein-protein network analysis performed on proteins with a MiST score >0.90 using an interaction score of 0.4 (medium).

Statistical analysis

Statistical tests for flow cytometry data were performed using GraphPad Prism software. A p-value of <0.05 was considered significant in these analyses. Student's *t*-test (two-tailed) was used for comparisons between two independent conditions. Paired Student's *t*-test was used when the samples being compared originated from the same animal.

Code and data availability

RNA-seq, ATAC-seq, and ChIP-seq data have been deposited in the NCBI Gene Expression Omnibus (GEO) database and are accessible through the GEO SuperSeries accession number: GSE131871. Custom code used for RNA-seq and ATAC-seq analysis are available at the GitHub links provided above. All other relevant data are available from the corresponding author upon reasonable request.

Supplementary Material

Refer to Web version on PubMed Central for supplementary material.

Extended Data

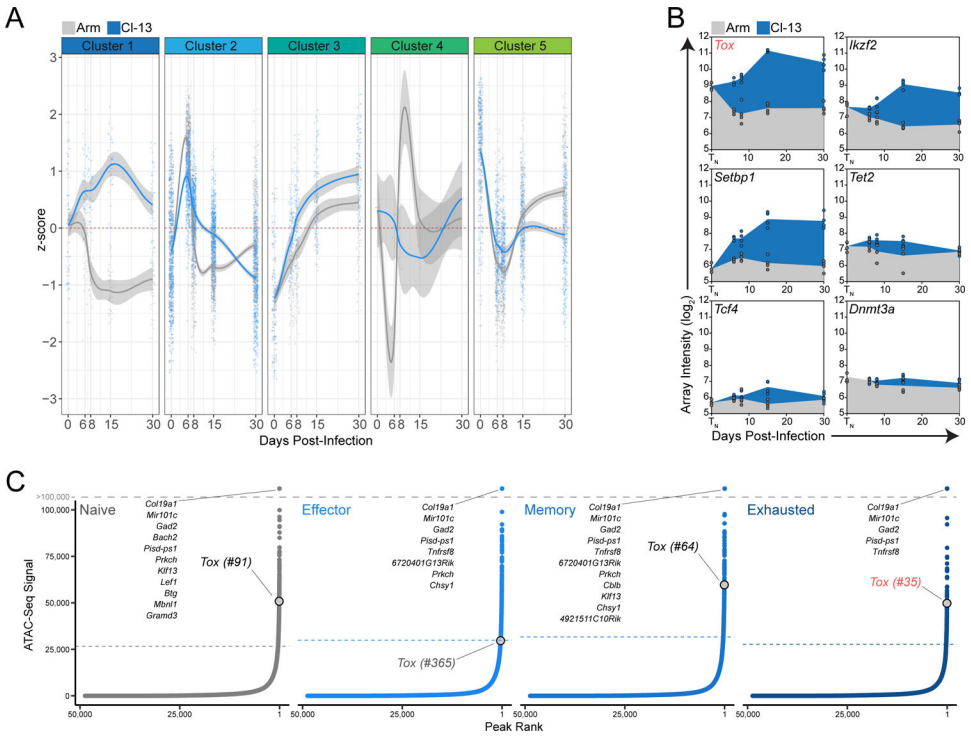

Extended Data Figure 1.

(A) Data points indicate the z-score of each gene in clusters 1–5 plotted against time post-Arm or Cl-13 infection. Gray and blue lines represent the moving average of z-score with 95% confidence interval in P14 cells from Arm and Cl-13 infection, respectively. **(B)** Expression of selected genes within cluster 1 plotted as normalized array intensity against time p.i. Gray and blue represent P14 cells from Arm and Cl-13 infection, respectively. **(C)** Distribution of ATAC-seq signal across loci in T_N, T_{EFF}, T_{MEM}, and T_{EX} P14 T cells. Loci above horizontal dashed lines denote putative super enhancers. Rank of the *Tox* locus among all identified potential super enhancers is shown.

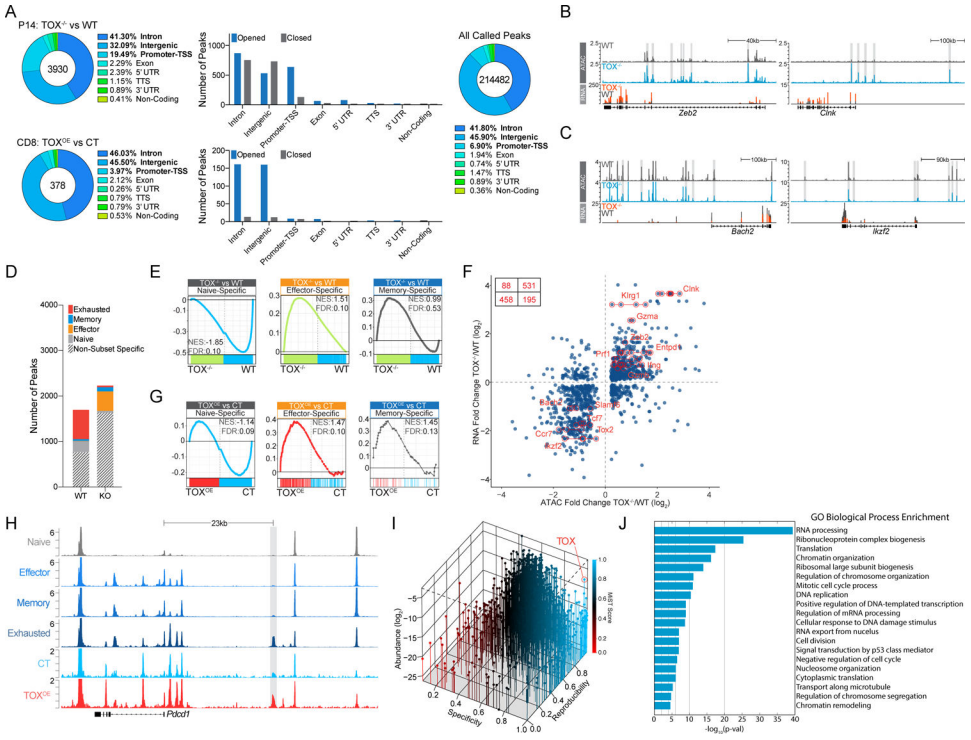

Extended Data Figure 2.

(A) TOX expression in P14 cells from peripheral blood at d208 p.i. with Arm or Cl-13. **(B)** T_{EFF} and T_{MEM} markers relative to TOX expression in P14 T cells or endogenous $CD8^+$ T cells on d6 post-Cl-13 infection (top). Frequency of T_{MEM} and T_{EFF} subsets within TOX^+ and TOX^- P14 T cell populations (bottom left). TOX median fluorescence intensity in KLRG1+ and KRLG1- P14 cells (bottom right). **(C)** TOX versus TF expression following 8 or 30 days of Cl-13 infection. **(D,E)** TOX versus IR expression in P14 cells following 8 (D) or 30 days (E) of Cl-13 infection. **(F)** TOX expression in antigen specific $CD8^+$ T cells following influenza, VSV, or *Listeria monocytogenes* infection compared with LCMV Arm or Cl-13. **(G)** TOX versus PD-1 and quantification of TOX expression in activated $CD8^+$ $CD44^+$ T cells from control tissues or tumors. Control T cells for mouse tumor models were acquired from the spleen, whereas in humans, T cells from the peripheral blood of normal donors served as controls. **(H)** Radar plots of median gene expression in single cell RNA sequencing data from tumor biopsies and peripheral blood of patients with non-small cell lung cancer (NSCLC) or hepatocellular carcinoma (HCC)[63,64]. Median expression was calculated on cell clusters that were defined by key driver genes and represent canonical T cell populations[63,64]. **(I)** P14 T cell infiltration in GP33-expressing B16 tumors (top). Cytokine production in TOX^+ or TOX^- tumor-infiltrating P14 cells (bottom). Contour and histogram plots are from one representative experiment of at least 2 independent experiments consisting of ≥4 mice per group. Unless otherwise noted, P14 cells were analyzed from the spleens of infected animals. Summarized experiments denote one animal per data point and error is reported as standard deviation (SD). For (E), 5 human melanoma biopsy samples were analyzed. Statistical significance (*P<0.01, **P<0.001, ***P<0.0001) determined by Student's *t*-test.

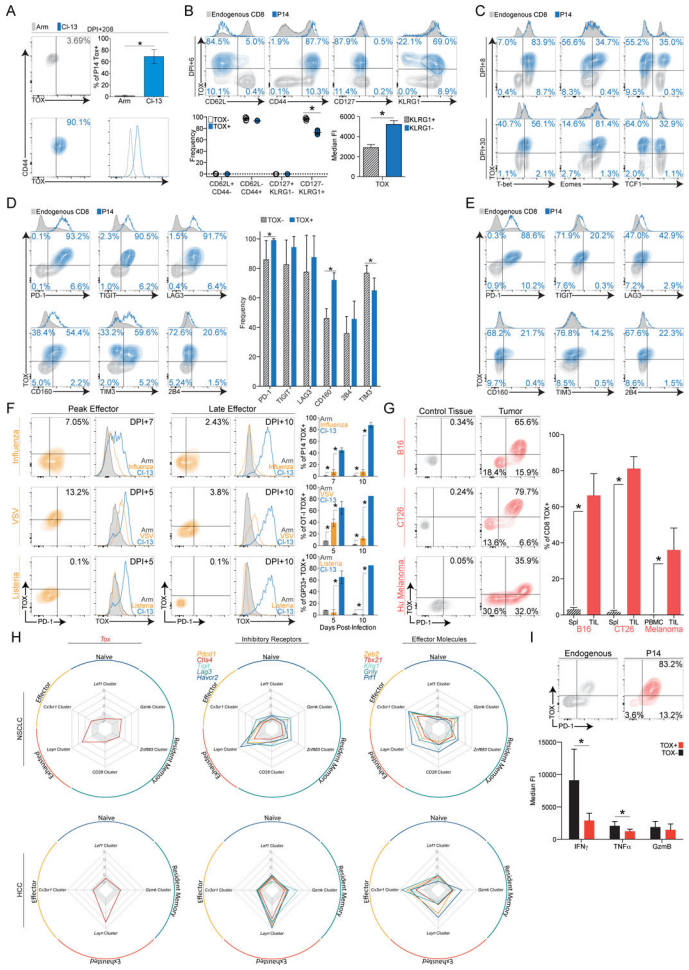

Extended Data Figure 3.

(A) Gating strategy used in co-adoptive transfer and infection experiments. **(B)** Expression of activation markers and TFs in naïve WT and $Tox^{Flox/Flox}$ $CD4^{Cre}$ P14 cells prior to adoptive transfer. WT and TOX cKO T cells were mixed 1:1 and adoptively transferred into congenic WT mice followed by infection with Arm (C,D,F-K) or Cl-13 (C-E). **(C)** Frequency of WT or TOX cKO P14 cells during Arm or Cl-13 infection. **(D)** TOX expression in WT and TOX cKO P14 T cells following Arm or Cl-13 infection. **(E)** Ki-67 expression on d8 of Cl-13 infection. **(F,G)** Frequency of memory populations on d8 (F) or d30 (G) of Arm infection. **(H)** TF expression in WT and TOX cKO P14 T cells on d30 p.i. with Arm. **(I-K)** Cytokine and effector molecule (I), IR (J), and TF (K) expression on d8 p.i. with Arm. IR expression reported as the ratio of the MFI between TOX cKO and WT P14 T cells (J, right). **(L)** GSEA of transcriptional signatures associated with T_N or T_{MEM} compared to the differentially expressed genes in $TOX^{-/-}$ versus WT P14 cells. **(M)** Expression of genes associated with terminal short-lived T_{EFF} subset[27]. **(N)** Comparison of transcriptional signature of TOX cKO and TCF1 cKO[31] T cells following eight days of Cl-13 infection. Genes differentially expressed relative to WT (FDR<0.05 and log-fold change >0.6) were compared between datasets. Contour and histogram plots are representative of ≥4 independent experiments with ≥4 mice. Statistical significance

(*P<0.01, **P<0.001, ***P<0.0001) determined by pair-wise *t*-test with Holm-Sidak correction (C) or Student's *t*-test (E-L), error reported as SD.

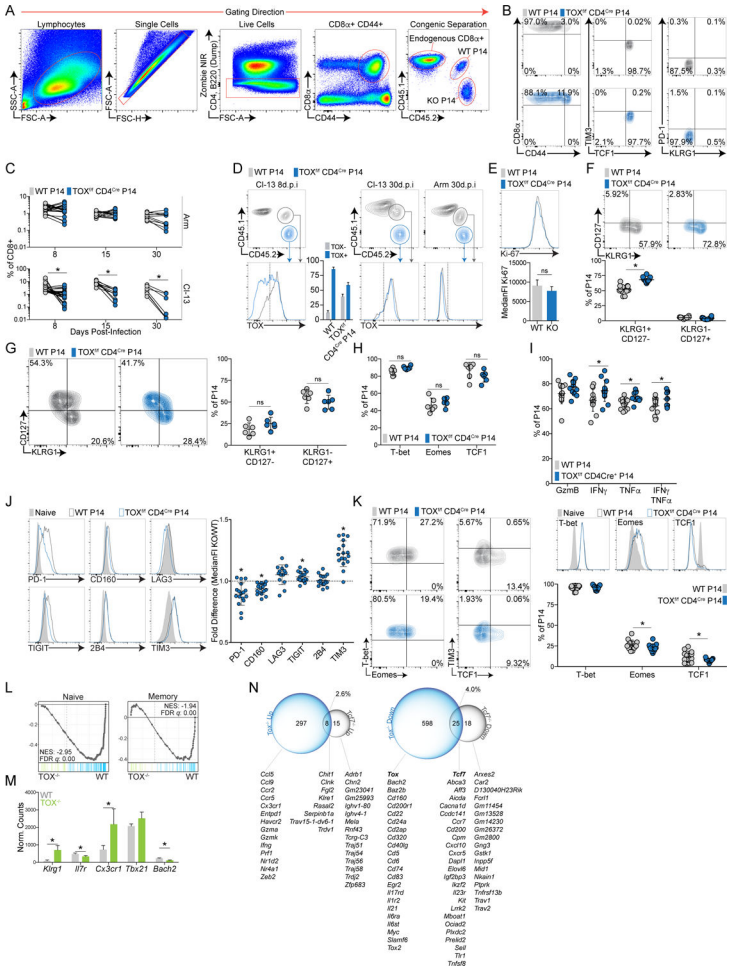

Extended Data Figure 4.

(A) Normalized microarray expression of *Nfatc1* (encodes NFAT2) and *Nfatc2* (encodes NFAT1) in P14 T cells following Arm or Cl-13 infection. **(B)** $CD8^+$ T cells were enriched, activated, and transduced with CT, WT-NFAT2, or CA-NFAT2 encoding RVs. T cells were expanded and differentiated *in vitro* in the presence of IL-2 for 6 days prior to analysis. **(C)** Expression of activation markers and TFs in naïve WT and $NFAT2^{Flox/Flox}$ $CD4^{Cre}$ P14 cells from the blood prior to adoptive transfer. **(D)** P14 T cells were adoptively transferred into WT hosts followed by infection with Cl-13. On d3–7 of infection, mice were treated with PBS or FK506 and splenocytes were harvested on d8 p.i. (top). CD44 expression in P14 T cells on d8 following infection with Cl-13 and treatment with PBS or FK506 on d3–7 (bottom). **(E)** NFAT2 cKO $CD8^+$ T cells were enriched from naïve mice, activated with αCD3 and αCD28 and transduced with RVs encoding TOX or GFP only control. 24 hours later, cells were sorted and transferred into Cl-13 infected mice. Protein expression analyzed on d8 p.i. **(F)** P14 T cells were transferred into WT mice followed by infection with Cl-13. On d25–29 p.i., recipient mice were treated with PBS, FK506, or CsA and splenocytes were harvested on d30 p.i. for analysis. **(G)** Protein expression in P14 cells following treatment with CsA or PBS on d25–29 of Cl-13 infection. All contour and histogram plots are representative of ≥3 independent experiments consisting of ≥3 mice per group. Statistical

significance (*P<0.01, **P<0.001, ***P<0.0001) determined by Student's *t*-test, error reported as SD.

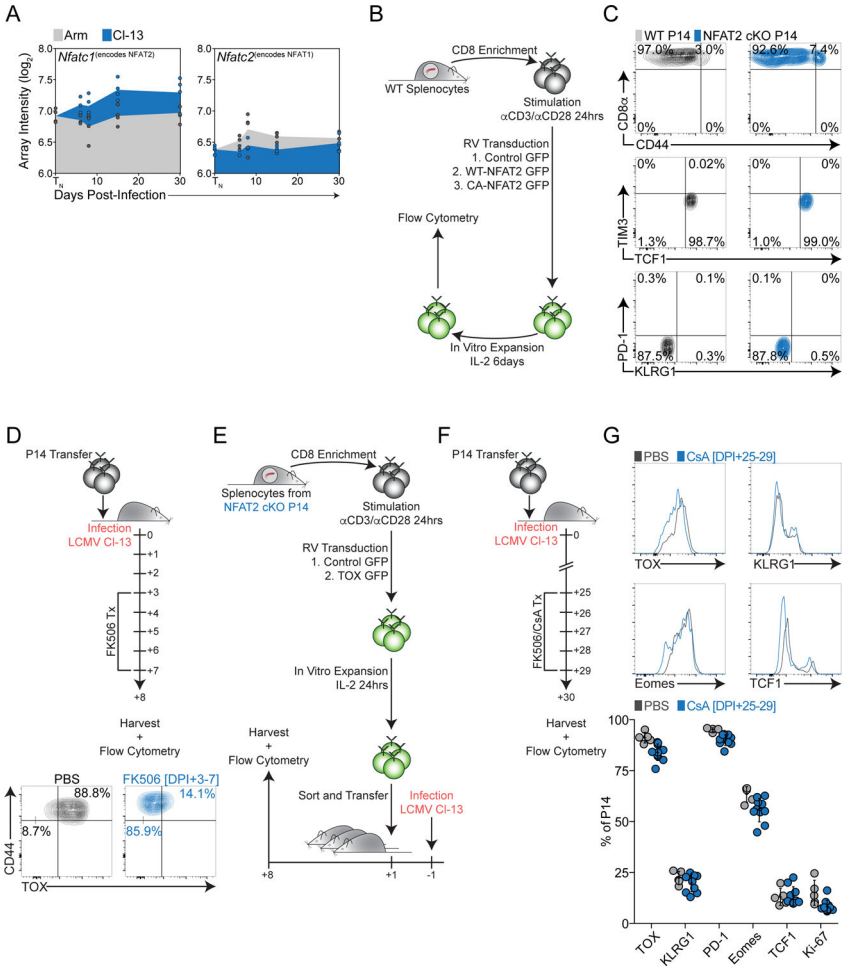

Extended Data Figure 5.

(A-D) Naïve P14 T cells were activated with αCD3 and αCD28 antibodies for 24 hours prior to transduction with RVs encoding TOX (TOX^{OE}) or control GFP (CT). Twenty-four hours following transduction, GFP^+ cells were sorted and transferred into d2 Arm-infected recipients. Eight days following transfer, transduced P14 cells were isolated from spleens and assayed for **(A)** $KLRG1^+$ T_{EFF} frequency, **(B)** IR expression, **(C)** cytokine production following 5 hours of restimulation with $GP^{33–41}$ peptide, and **(D)** TF expression. **(E,F)** Distribution of memory T cell subsets and PD-1 expression in TOX versus CT transduced P14 cells following 30 days of Arm infection. **(G)** Genes upregulated (blue) or downregulated (gray) in TOX^{OE} versus CT cells were analyzed for enrichment in the transcripts differentially expressed in P14 from *in vivo* Arm versus Cl-13 at d8, 15, and 30 p.i.[13]. Normalized GSEA enrichment scores (NES) plotted versus time p.i. **(H)** Experimental procedure used to generate datasets analyzed in Fig.5e,f and Extended Data Fig.5i,j. NIH3T3 cells were transduced with RVs encoding TOX+GFP (TOX^{OE}) or control GFP only (CT). Cells were cultured for 48 hours, then harvested and processed for RNA-seq analysis. **(I)** GO analysis of biological processes differentially regulated in TOX^{OE} versus CT fibroblasts. **(J)** As in (G), genes upregulated (blue) or downregulated (gray) in fibroblasts were assayed for enrichment in the genes differentially expressed in P14 cells on d6, 8, 15,

and 30 of Arm or Cl-13 infection[13]. All contour and histogram plots are representative of ≥2 independent experiments consisting of ≥5 mice per group. Unless otherwise noted, P14 cells were analyzed from the spleens of infected animals. Statistical significance (*P<0.01, **P<0.001, ***P<0.0001) determined by Student's *t*-test, error reported as SD.

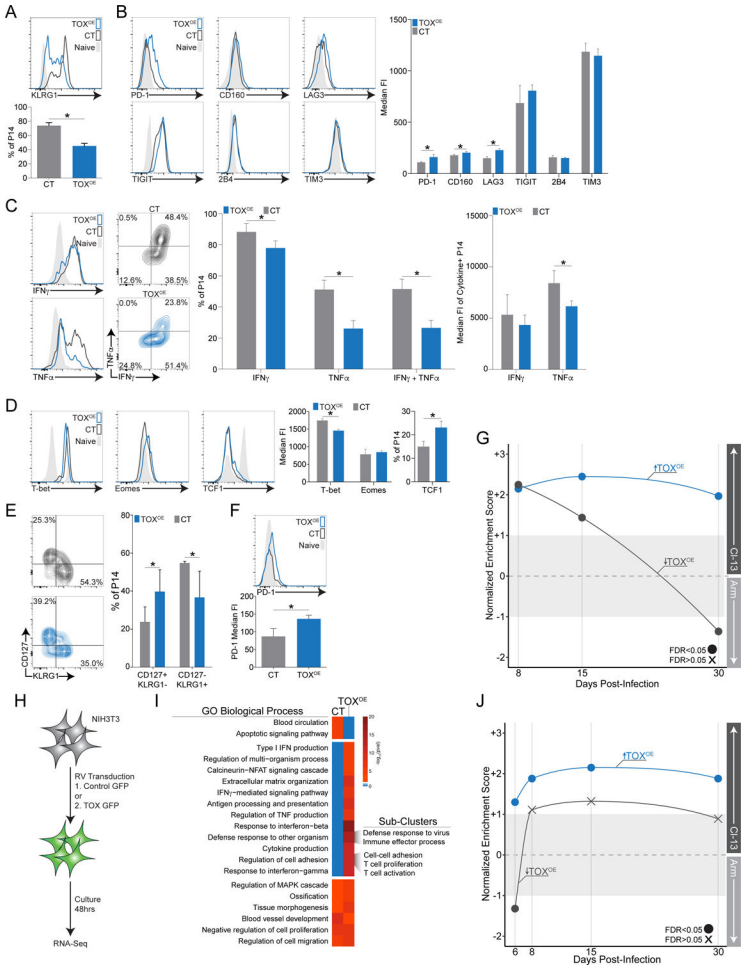

Extended Data Figure 6.

(A) Location of differentially accessible ATAC-seq peaks from Fig. 6A (top left) or Fig. 6F (bottom right). Right, distribution of all peaks in $CD8^+$ T cells above background levels. (**B**,**C**) ATAC-seq and RNA-seq tracks of T_{EFF} (B) or T_{MEM} (C) -associated loci. Peaks uniquely opened (B) or closed (C) in $TOX^{-/-}$ relative to WT T cells are highlighted with gray bars. (**D**) Enumeration of significantly differentially accessible sites (FDR<0.05) in WT and $TOX^{-/-}$ T cells at T_{EX}-specific and T_{EFF}-specific loci[14]. (**E**) PSEA of chromatin regions specifically accessible in $T_{N,}$ T_{EFF}, T_{MEM}[14] in $TOX^{-/-}$ versus WT P14. **(F)** Fold change in ATAC accessibility versus RNA expression. Key T_{EX} and T_{EFF} genes are highlighted and genes associated with multiple peaks are connected with a red line. Inset table enumerates the number of gene-ATAC peak pairs in each quadrant. (**G**) PSEA of chromatin regions specifically accessible in $T_{N,}$ T_{EFF}, T_{MEM} in TOX^{OE} versus CT P14. **(H)** ATAC-seq tracks of T_N, T_{EFF}, T_{MEM}, and T_{EX} cells[14] compared with CT and TOX^{OE} T cells at the *Pdcd1* locus. Gray bar highlights the T_{EX}-specific −23.8kb enhancer. (**I**) Abundance, specificity and reproducibility plot of proteins identified by MS analysis following TOX immunoprecipitation versus IgG control in EL4 cells. Hits are colored by MiST score (blue signifies >0.75). (**J**) GO biological process enrichment of TOX-bound proteins identified in (I) with MiST score >0.75.

ACKNOWLEDGEMENTS

We thank all members of the Wherry lab for helpful discussions and critical analysis of the manuscript. We thank J. Kaye for providing the $TOX^{Flox/Flox}$ and $TOX^{-/-}$ mice used in this study. We would also like to thank P.M. Porrett for providing FK506. We also thank D. Zehn for helpful discussions. Additionally, the authors would like to thank Dr. Hsin-Yao Tang and Thomas Beer of the Wistar Institute Proteomics and Metabolomics Facility for their assistance on the analysis of the proteomics data. Support of the Wistar Proteomics and Metabolomics Core Facility was provided by Cancer Center Support Grant CA010815 to the Wistar Institute. OK was supported by an NIAID F30 fellowship (F30AI129263). This work was funded by the National Institutes of Health (AI105343, AI082630, AI115712, CA210944, AI117950, AI108545) and the Parker Institute for Cancer Immunotherapy. E.J.W has a patent licensing agreement on the PD-1 pathway.

REFERENCES

1. Kaech SM & Cui W Transcriptional control of effector and memory CD8+ T cell differentiation. Nat Rev Immunol 12, 749–761 (2012). [PubMed: 23080391]
2. Wherry EJ & Kurachi M Molecular and cellular insights into T cell exhaustion. Nat Rev Immunol 15, 486–499 (2015). [PubMed: 26205583]
3. Barber DL et al. Restoring function in exhausted CD8 T cells during chronic viral infection. Nature 439, 682–687 (2005). [PubMed: 16382236]
4. Frebel H et al. Programmed death 1 protects from fatal circulatory failure during systemic virus infection of mice. J Exp Med 209, 2485–2499 (2012). [PubMed: 23230000]
5. Zajac AJ et al. Viral Immune Evasion Due to Persistence of Activated T Cells Without Effector Function. J Exp Med 188, 2205–2213 (1998). [PubMed: 9858507]
6. Gallimore A et al. Induction and Exhaustion of Lymphocytic Choriomeningitis Virus–specific Cytotoxic T Lymphocytes Visualized Using Soluble Tetrameric Major Histocompatibility Complex Class I–Peptide Complexes. J Exp Med 187, 1383–1393 (1998). [PubMed: 9565631]
7. Lechner F et al. Analysis of Successful Immune Responses in Persons Infected with Hepatitis C Virus. J Exp Med 191, 1499–1512 (2000). [PubMed: 10790425]
8. Shankar P et al. Impaired function of circulating HIV-specific CD8(+) T cells in chronic human immunodeficiency virus infection. Blood 96, 3094–3101 (2000). [PubMed: 11049989]
9. Pauken KE & Wherry EJ Overcoming T cell exhaustion in infection and cancer. Trends in Immunology 36, 265–276 (2015). [PubMed: 25797516]
10. Page DB, Postow MA, Callahan MK, Allison JP & Wolchok JD Immune Modulation in Cancer with Antibodies. Annu. Rev. Med 65, 185–202 (2014). [PubMed: 24188664]
11. Hirano F et al. Blockade of B7-H1 and PD-1 by monoclonal antibodies potentiates cancer therapeutic immunity. Cancer Res 65, 1089–1096 (2005). [PubMed: 15705911]
12. Barber DL et al. Restoring function in exhausted CD8 T cells during chronic viral infection. Nature 439, 682–687 (2005). [PubMed: 16382236]
13. Doering TA et al. Network Analysis Reveals Centrally Connected Genes and Pathways Involved in CD8+ T Cell Exhaustion versus Memory. Immunity 37, 1130–1144 (2012). [PubMed: 23159438]
14. Pauken KE et al. Epigenetic stability of exhausted T cells limits durability of reinvigoration by PD-1 blockade. Science 354, 1160–1165 (2016). [PubMed: 27789795]
15. Sen DR et al. The epigenetic landscape of T cell exhaustion. Science 354, 1165–1169 (2016). [PubMed: 27789799]
16. Scott-Browne JP et al. Dynamic Changes in Chromatin Accessibility Occur in CD8+ T Cells Responding to Viral Infection. Immunity 45, 1327–1340 (2016). [PubMed: 27939672]
17. Philip M et al. Chromatin states define tumour-specific T cell dysfunction and reprogramming. Nature 545, 452–456 (2017). [PubMed: 28514453]
18. Lara-Astiaso D et al. Immunogenetics. Chromatin state dynamics during blood formation. Science 345, 943–949 (2014). [PubMed: 25103404]
19. Carty SA et al. The Loss of TET2 Promotes CD8+ T Cell Memory Differentiation. J Immunol 200, 82–91 (2018). [PubMed: 29150566]

20. Ghoneim HE et al. De Novo Epigenetic Programs Inhibit PD-1 Blockade- Mediated T Cell Rejuvenation. Cell 170, 142–157.e19 (2017). [PubMed: 28648661]
21. Aliahmad P, Seksenyan A & Kaye J The many roles of TOX in the immune system. Current Opinion in Immunology 24, 173–177 (2012). [PubMed: 22209117]
22. Seehus CR et al. The development of innate lymphoid cells requires TOX-dependent generation of a common innate lymphoid cell progenitor. Nat Immunol 16, 599–608 (2015). [PubMed: 25915732]
23. Whyte WA et al. Master Transcription Factors and Mediator Establish Super-Enhancers at Key Cell Identity Genes. Cell 153, 307–319 (2013). [PubMed: 23582322]
24. Hnisz D et al. Super-Enhancers in the Control of Cell Identity and Disease. Cell 155, 934–947 (2013). [PubMed: 24119843]
25. Wherry EJ, Blattman JN, Murali-Krishna K, van der Most R & Ahmed R Viral Persistence Alters CD8 T-Cell Immunodominance and Tissue Distribution and Results in Distinct Stages of Functional Impairment. J Virol 77, 4911–4927 (2003). [PubMed: 12663797]
26. Joshi NS et al. Inflammation directs memory precursor and short-lived effector CD8(+) T cell fates via the graded expression of T-bet transcription factor. Immunity 27, 281–295 (2007). [PubMed: 17723218]
27. Herndler-Brandstetter D et al. KLRG1+ Effector CD8+ T Cells Lose KLRG1, Differentiate into All Memory T Cell Lineages, and Convey Enhanced Protective Immunity. Immunity 48, 716–729.e8 (2018). [PubMed: 29625895]
28. Angelosanto JM, Blackburn SD, Crawford A & Wherry EJ Progressive Loss of Memory T Cell Potential and Commitment to Exhaustion during Chronic Viral Infection. J Virol 86, 8161–8170 (2012). [PubMed: 22623779]
29. Paley MA et al. Progenitor and Terminal Subsets of CD8+ T Cells Cooperate to Contain Chronic Viral Infection. Science 338, 1220–1225 (2012). [PubMed: 23197535]
30. Utzschneider DT et al. T Cell Factor 1-Expressing Memory-like CD8+ T Cells Sustain the Immune Response to Chronic Viral Infections. Immunity 45, 415–427 (2016). [PubMed: 27533016]
31. Wu T et al. The TCF1-Bcl6 axis counteracts type I interferon to repress exhaustion and maintain T cell stemness. Sci Immunol 1, eaai8593–eaai8593 (2016). [PubMed: 28018990]
32. Joshi NS et al. Inflammation directs memory precursor and short-lived effector CD8(+) T cell fates via the graded expression of T-bet transcription factor. Immunity 27, 281–295 (2007). [PubMed: 17723218]
33. Aliahmad P et al. TOX Provides a Link Between Calcineurin Activation and CD8 Lineage Commitment. J Exp Med 199, 1089–1099 (2004). [PubMed: 15078895]
34. Macian F NFAT proteins: key regulators of T-cell development and function. Nat Rev Immunol 5, 472–484 (2005). [PubMed: 15928679]
35. Martinez GJ et al. The Transcription Factor NFAT Promotes Exhaustion of Activated CD8+ T Cells. Immunity 42, 265–278 (2015). [PubMed: 25680272]
36. Klein-Hessling S et al. NFATc1 controls the cytotoxicity of CD8+ T cells. Nature Communications 1–15 (2017). doi:10.1038/s41467-017-00612-6
37. Monticelli S & Rao A NFAT1 and NFAT2 are positive regulators of IL-4 gene transcription. Eur. J. Immunol 32, 2971–2978 (2002). [PubMed: 12355451]
38. Bengsch B et al. Epigenomic-Guided Mass Cytometry Profiling Reveals Disease-Specific Features of Exhausted CD8 T Cells. Immunity 48, 1029–1045.e5 (2018). [PubMed: 29768164]
39. Johnson JL et al. Lineage-Determining Transcription Factor TCF-1 Initiates the Epigenetic Identity of T Cells. Immunity 48, 243–257.e10 (2018). [PubMed: 29466756]
40. Lalonde ME et al. Exchange of associated factors directs a switch in HBO1 acetyltransferase histone tail specificity. Genes & Development 27, 2009–2024 (2013). [PubMed: 24065767]
41. Miotto B & Struhl K HBO1 Histone Acetylase Activity Is Essential for DNA Replication Licensing and Inhibited by Geminin. Molecular Cell 37, 57–66 (2010). [PubMed: 20129055]
42. Yu B et al. Epigenetic landscapes reveal transcription factors that regulate CD8+ T cell differentiation. Nat Immunol 18, 573–582 (2017). [PubMed: 28288100]

43. Boiani M & Schöler HR Regulatory networks in embryo-derived pluripotent stem cells. Nat Rev Mol Cell Biol 6, 872–884 (2005). [PubMed: 16227977]
44. Iwai Y, Terawaki S & Honjo T PD-1 blockade inhibits hematogenous spread of poorly immunogenic tumor cells by enhanced recruitment of effector T cells. Int. Immunol 17, 133–144 (2005). [PubMed: 15611321]
45. Strome SE et al. B7-H1 blockade augments adoptive T-cell immunotherapy for squamous cell carcinoma. Cancer Res 63, 6501–6505 (2003). [PubMed: 14559843]
46. Blank C et al. PD-L1/B7H-1 inhibits the effector phase of tumor rejection by T cell receptor (TCR) transgenic CD8+ T cells. Cancer Res 64, 1140–1145 (2004). [PubMed: 14871849]
47. Anderson KL et al. Transcription Factor PU.1 Is Necessary for Development of Thymic and Myeloid Progenitor-Derived Dendritic Cells. J Immunol 164, 1855–1861 (2000). [PubMed: 10657634]
48. Fontenot JD, Gavin MA & Rudensky AY Foxp3 programs the development and function of CD4+CD25+ regulatory T cells. Nat Immunol 4, 330–336 (2003). [PubMed: 12612578]
49. Hori S, Nomura T & Sakaguchi S Control of regulatory T cell development by the transcription factor Foxp3. Science 299, 1057–1061 (2003). [PubMed: 12522256]
50. Weber BN et al. A critical role for TCF-1 in T-lineage specification and differentiation. Nature 476, 63–68 (2011). [PubMed: 21814277]

METHODS REFERENCES

51. Aliahmad P & Kaye J Development of all CD4 T lineages requires nuclear factor TOX. J Exp Med 205, 245–256 (2008). [PubMed: 18195075]
52. Blattman JN, Wherry EJ, Ha SJ, van der Most RG & Ahmed R Impact of Epitope Escape on PD-1 Expression and CD8 T-Cell Exhaustion during Chronic Infection. J Virol 83, 4386–4394 (2009). [PubMed: 19211743]
53. Odorizzi PM, Pauken KE, Paley MA, Sharpe A & Wherry EJ Genetic absence of PD-1 promotes accumulation of terminally differentiated exhausted CD8+ T cells. J Exp Med 212, 1125–1137 (2015). [PubMed: 26034050]
54. Araki K et al. Pathogenic virus-specific T cells cause disease during treatment with the calcineurin inhibitor FK506: implications for transplantation. J Exp Med 207, 2355–2367 (2010). [PubMed: 20921283]
55. Kurachi M et al. Optimized retroviral transduction of mouse T cells for in vivo assessment of gene function. Nat Protoc 12, 1980–1998 (2017). [PubMed: 28858287]
56. Huang AC et al. T-cell invigoration to tumour burden ratio associated with anti-PD-1 response. Nature 545, 60–65 (2017). [PubMed: 28397821]
57. Medvedeva YA et al. EpiFactors: a comprehensive database of human epigenetic factors and complexes. Database 2015, bav067–10 (2015). [PubMed: 26153137]
58. Shi J et al. Discovery of cancer drug targets by CRISPR-Cas9 screening of protein domains. Nat Biotechnol 33, 661–667 (2015). [PubMed: 25961408]
59. Buenrostro JD, Giresi PG, Zaba LC, Chang HY & Greenleaf WJ Transposition of native chromatin for fast and sensitive epigenomic profiling of open chromatin, DNA-binding proteins and nucleosome position 10, 1213–1218 (2013).
60. Dou Z et al. Autophagy mediates degradation of nuclear lamina. Nature 527, 105–109 (2015). [PubMed: 26524528]
61. Dawson MA et al. Inhibition of BET recruitment to chromatin as an effective treatment for MLL-fusion leukaemia. Nature 478, 529–533 (2011). [PubMed: 21964340]
62. Jäger S et al. Global landscape of HIV-human protein complexes. Nature 481, 365–370 (2012).
63. Guo X et al. Global characterization of T cells in non-small-cell lung cancer by single-cell sequencing. Nature Medicine 1–17 (2018). doi:10.1038/s41591-018-0045-3
64. Zheng C et al. Landscape of Infiltrating T Cells in Liver Cancer Revealed by Single-Cell Sequencing. Cell 169, 1342–1356.e16 (2017). [PubMed: 28622514]

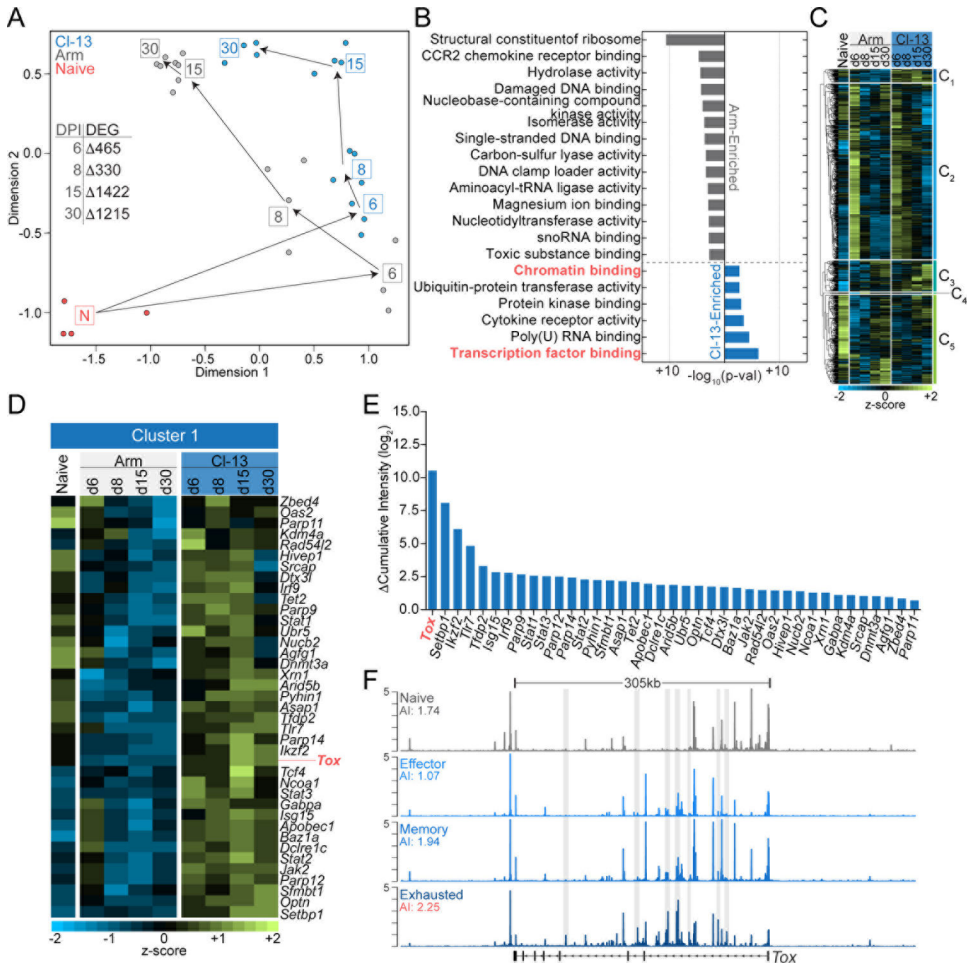

Figure 1 - Multiple epigenetic modulators, including TOX are selectively expressed in T_{EX}

(A) Multidimensional scaling analysis of transcriptional data from naive LCMV-specific P14 $CD8^+$ T cells (orange) or from acute (Arm, gray) or chronic (Cl-13, blue) LCMV at indicated days post-infection (p.i.). Inset table enumerates differentially expressed genes (FDR <0.05) between Arm and Cl-13 at specified days p.i. **(B)** Gene ontology (GO) analysis of differentially expressed genes 6 days post-Arm or Cl-13 infection. Gray and blue denote GO molecular functions enriched in Arm and Cl-13, respectively. Categories that include chromatin binding proteins are highlighted in red. **(C)** Heatmap of differentially expressed chromatin modulating genes (Supplementary Table 8, see methods) between naïve P14 T cells and among P14 T cells during Arm or Cl-13 infection. Genes are ordered by hierarchical clustering using Manhattan distance and clusters generated by k-means. Z-scores of $\log_2$ expression data shown. **(D)** Chromatin modulating genes in cluster 1. **(E)** Difference in cumulative expression of genes in cluster 1. Values were calculated by summing the normalized array intensity of each gene at all time points p.i. and subtracting Arm from Cl-13. **(F)** ATAC-seq tracks of *in vivo* T_N, T_{EFF}, T_{MEM} and T_{EX} P14 cells at the *Tox* locus. Accessibility Index (AI) of each sample calculated by summing the normalized tag counts across the locus and dividing by its length.

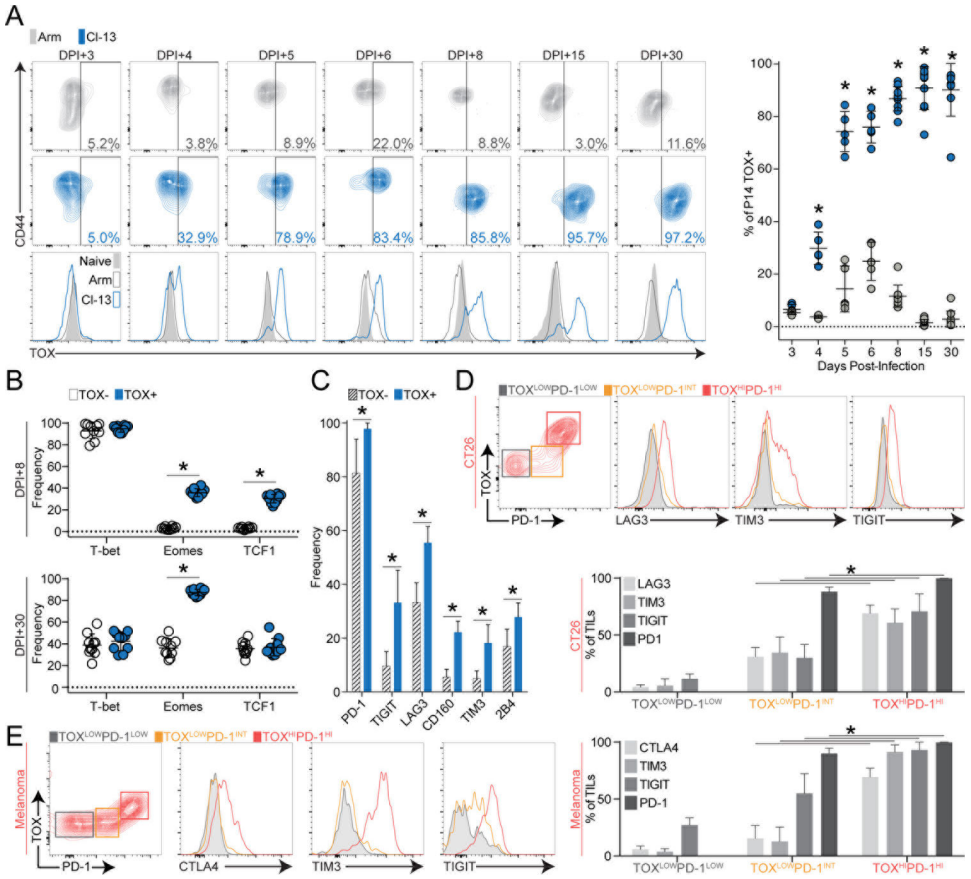

Figure 2 - Rapid and sustained TOX expression is associated with key features of exhaustion

(A) TOX protein expression in P14 T cells following Arm or Cl-13 infection. Frequencies of TOX^+ P14 cells relative to total P14 population (left) and summary data (right). **(B)** Transcription factor expression within TOX^+ and TOX^- P14 populations at d8 or d30 p.i. of Cl-13 infection. **(C)** Inhibitory receptor expression in TOX^+ and TOX^- P14 cells 30 days post-Cl-13 infection. **(D,E)** Identification of TOX-expressing cells in tumor-infiltrating $CD8^+$ T cells (TILs) from (**D**) CT26 carcinoma mouse model and (**E**) human melanoma biopsy samples. TOX versus PD-1 expression, inhibitory receptor expression in $TOX^{LOW}PD\text{-}1^{LOW}$, $TOX^{LOW}PD\text{-}1^{INT}$, and $TOX^{HI}PD\text{-}1^{HI}$ TIL populations, and summarized expression of IRs in these three populations. Contour and histogram plots representative of ≥3 independent experiments consisting of ≥4 mice. Unless otherwise noted, P14 cells were analyzed from the spleens of infected animals. Summarized experiments denote one animal per data point and error is reported as standard deviation (SD). For (E), 5 human TIL and 11 human normal donor samples were analyzed. Statistical significance (*P<0.01, **P<0.001, ***P<0.0001) determined by Student's *t*-test.

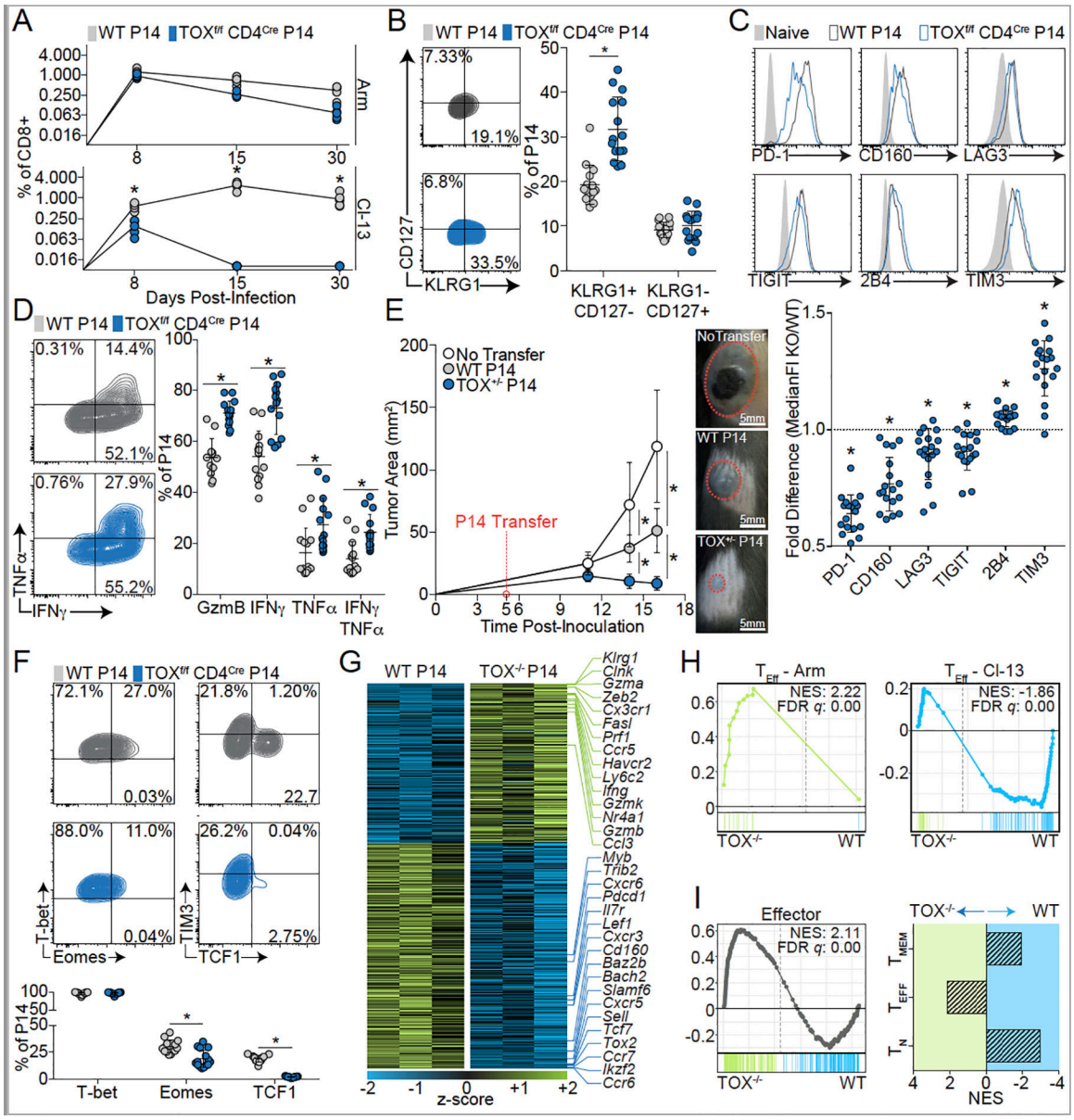

Figure 3 - TOX is required for the development of T_{EX}

WT and $TOX^{Flox/Flox}$ $CD4^{Cre}$ (TOX cKO) P14 T cells were mixed 1:1 and adoptively transferred into hosts. Spleens harvested at indicated time points following Arm or Cl-13 infection (A) or on d8 of Cl-13 infection (B-D, F). **(A)** Frequency of WT or TOX cKO T cells relative to the total $CD8^+$ T cell pool during Arm (top) or Cl-13 (bottom) infection. **(B)** KLRG1 and CD127, (**C**) IR, and (**D**) cytokine expression in WT and TOX cKO P14. Ratio of IR median fluorescence intensity between TOX cKO and WT P14. **(E)** Tumor area following inoculation with B16-GP33 and transfer of pre-activated WT or $TOX^{+/-}$ P14 T cells. **(F)** TF expression in WT and TOX cKO P14. **(G-I)** WT and $TOX^{-/-}$ P14 mixed 1:1, transferred into WT hosts, and recovered from the spleen on d8 of Cl-13 infection for RNA-seq. **(G)** Differentially expressed genes in WT versus $TOX^{-/-}$ P14. Genes associated with T_{EFF} or T_{MEM} are labeled. Each column represents a biological replicate. **(H)** Gene set

enrichment analysis of the transcriptional signature from early (d8) T cell responses to acute (T_{EFF}-Arm, left) or chronic (T_{EFF}-Cl-13, right) infection in $TOX^{-/-}$ versus WT P14[13]. **(I)** GSEA and normalized enrichment scores (NES) of transcriptional signatures associated with T_N, T_{EFF}, or T_{MEM} compared to the differentially expressed genes in $TOX^{-/-}$ versus WT P14. Contour and histogram plots representative of ≥4 independent experiments consisting of ≥4 mice. Y-axis of GSEA plots represent enrichment score. Heatmaps generated using z-scores derived from log_2 tag counts. Statistical significance (*P<0.01, **P<0.001, ***P<0.0001) determined by Student's *t*-test, error reported as SD.

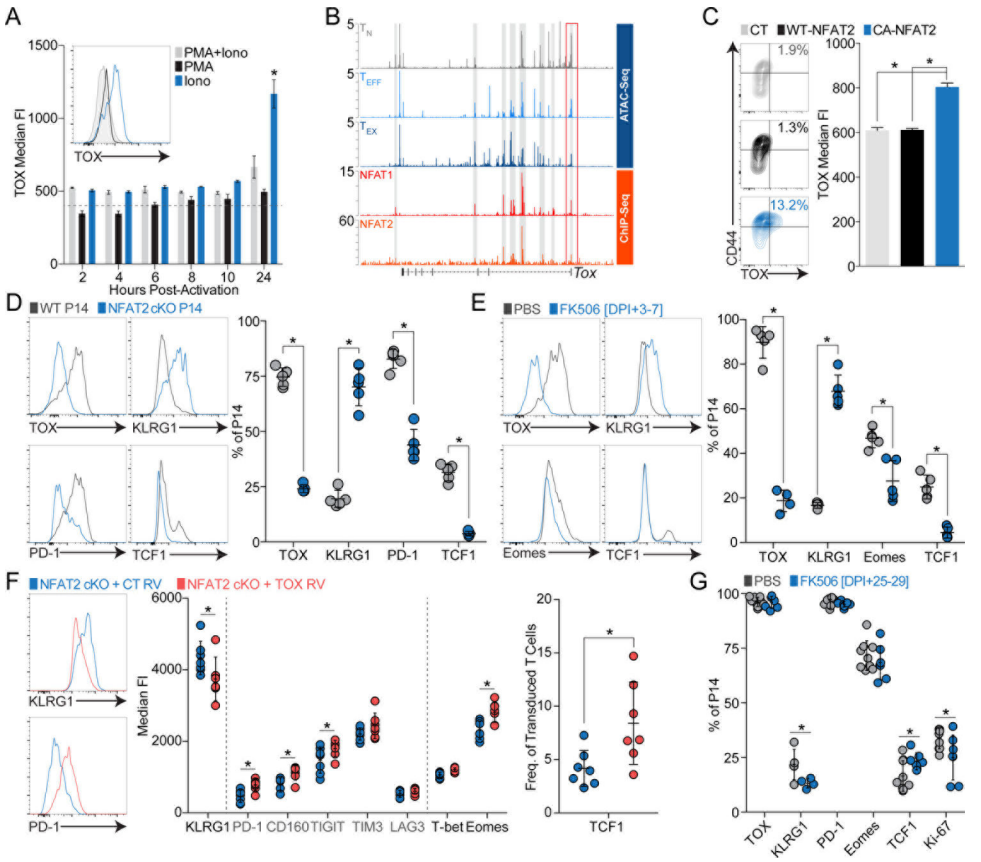

Figure 4 - Calcineurin signaling and NFAT2 are necessary and sufficient to induce TOX, but sustained expression becomes calcineurin independent

(A) TOX expression in $CD8^+$ T cells following 24 hours of stimulation with PMA, ionomycin, or PMA with ionomycin (inset). Time course of TOX MFI following addition of stimulus; dashed line indicates TOX MFI in T_N. **(B)** ATAC-seq tracks of the *Tox* locus in T_N, T_{EFF}, and T_{EX} P14 cells compared with NFAT1 (red) and NFAT2 (orange) ChIP-seq tracks from T_{EFF}[35,36]. Promoter region highlighted with red box. Gray bars highlight significant enrichment of NFAT1 and NFAT2. **(C)** TOX expression in WT-NFAT2, CA-NFAT2, or mock-transduced T cells. **(D)** WT and $NFAT2^{Flox/Flox}$ $CD4^{Cre}$ P14 T cells mixed 1:1 and adoptively transferred into WT hosts prior to infection with Cl-13. Frequency of TOX^+, $KLRG1^+$, $PD\text{-}1^+$, and $TCF1^+$ P14 cells on d8 p.i. **(E)** TOX, KLRG1, PD-1, and TCF1 expression in P14 on d8 p.i with Cl-13 following treatment with FK506 or PBS from d3–7. **(F)** NFAT2 cKO P14 cells were transduced with a RV encoding TOX (NFAT2 cKO + TOX) or control GFP (NFAT2 cKO + CT) and adoptively transferred into WT congenic mice infected with Cl-13. T_{EFF} markers, IRs, and TFs were evaluated on d7 p.i. **(G)** T_{EFF} marker, IR, and TF expression measured on d30 p.i. with Cl-13 following treatment with FK506 or PBS on d25–29. Contour and histogram plots are representative of ≥3 independent experiments consisting of ≥3 mice per group. Unless otherwise noted, P14 cells were analyzed from the spleens of infected animals. Statistical significance (*P<0.01, **P<0.001, ***P<0.0001) determined by Student's *t*-test, error reported as SD.

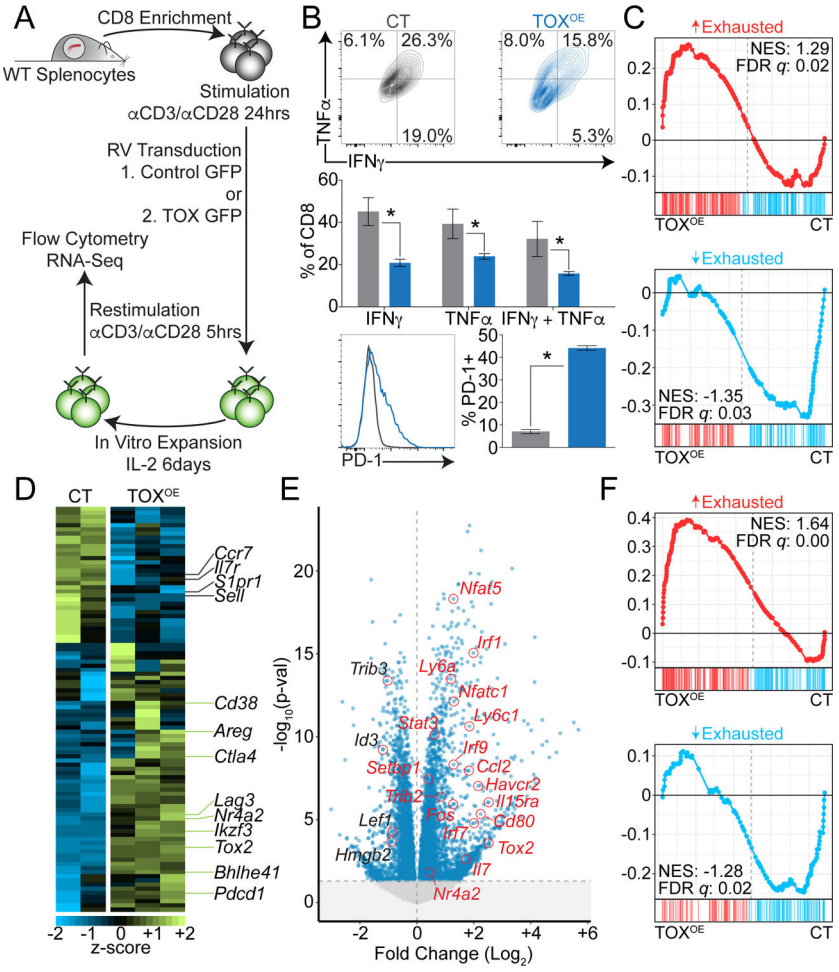

Figure 5 - TOX enforces a TEX transcriptional program

(A) Experimental procedure used in (B)-(D). $CD8^+$ T cells isolated from spleens, activated, transduced with RVs encoding TOX (TOX^{OE}) or control GFP (CT), and restimulated prior to analysis. **(B)** Cytokine and PD-1 expression following restimulation. **(C)** Genes uniquely upregulated (red) or downregulated (blue) in T_{EX}[38] were assayed for enrichment in TOX^{OE} or CT T cells using GSEA. **(D)** Heatmap of leading edge genes from (C). Key genes associated with T_{EX} are labeled. **(E)** Differentially expressed genes in TOX^{OE} relative to CT transduced fibroblasts. Transcripts with a FDR value <0.05 are highlighted in blue. T_{EX}-associated genes from the leading edge of (F) labeled in red. **(F)** As in (C), genes uniquely up-(red) or down-(blue) regulated in T_{EX} were analyzed for enrichment in TOX^{OE} versus CT transduced fibroblasts[38]. Contour and histogram plots are representative of ≥3 independent experiments. RNA-seq datasets were generated from ≥2 biological replicates. Heatmaps generated using z-scores derived from $\log_2$ tag counts. Y-axis of GSEA plots represent enrichment score (ES). Statistical significance (*P<0.01, **P<0.001, ***P<0.0001) determined by Student's *t*-test, error reported as SD.

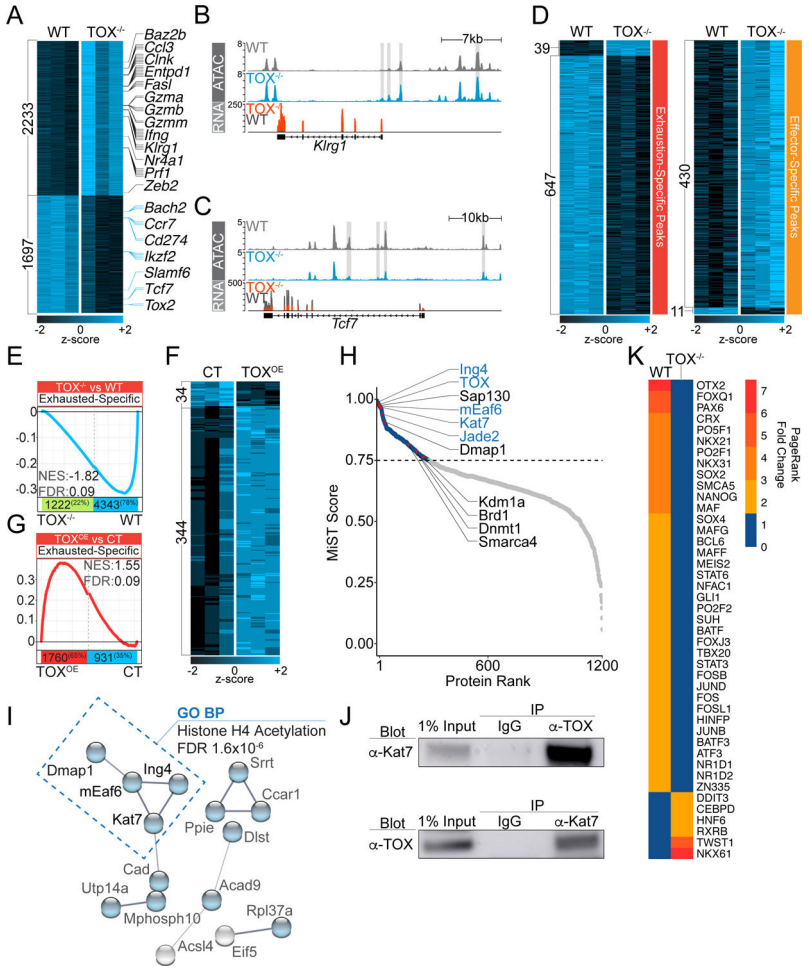

Figure 6 - TOX induces an epigenetic signature of TEX by recruiting the HBO1 complex

(**A-E**) ATAC-seq on TOX$^{-/-}$ and WT P14 T cells following 8 days of Cl-13 infection. (**A**) Differentially accessible loci. Regions proximal to T_{EFF} (black) and T_{MEM}/T_N (blue) genes are labeled. Lines denote number of gene-proximal loci with significant accessibility changes. Each column represents a biological replicate. ATAC-seq and RNA-seq tracks of T_{EFF} (**B**) or T_{MEM} (**C**) -associated loci. Differentially accessible sites are highlighted with gray bars. (**D**) Significantly differentially accessible sites (FDR<0.05) in WT and TOX$^{-/-}$ T cells at T_{EX}-specific and T_{EFF}-specific peaks[14]. (**E**) Chromatin regions specifically accessible in T_{EX}[14] were analyzed for enrichment in the TOX$^{-/-}$ versus WT P14 T cells by peak set enrichment analysis (PSEA). (**F,G**) ATAC-seq on *in vitro* T cells transduced with RV encoding TOX (TOX^{OE}) or control GFP (CT). (**F**) Differentially accessible chromatin regions in TOX^{OE} compared to CT cells. (**G**) PSEA of T_{EX}-specific loci as in (E) using differentially accessible loci in TOX^{OE} versus CT CD8^{+} T cells. (**H**) MiST score of proteins identified after TOX immunoprecipitation and mass spectrometry from EL4 lysate. Dashed line indicates high-confidence hits. (**I**) STRING network analysis of proteins with a MiST score >0.90. GO biological process (BP) analysis on subsequent network is highlighted. (**J**) αTOX used to immunoprecipitate from EL4 lysate and blotted with αKat7 (top). Reverse IP was performed by immunoprecipitating with αKat7, then blotting with αTOX (bottom). (**K**)

Heatmap of TFs with a PageRank score >1.5-fold different between WT and $TOX^{-/-}$ P14 on d8 of Cl-13. NFAC1 represents NFAT2. Heatmaps generated using z-scores derived from log_2 tag counts. Y-axis of PSEA plots represent enrichment score (ES).